technical memorandum Daresbury Laborato

DL/SCI/TM85E

CHARACTERISTICS OF TGM6

by

T.S. TURNER and D. TEEHAN, SERC Daresbury Laboratory

MARCH, 1992

G92/050

Science and Engineering Research Council
DARESBURY LABORATORY
Daresbury, Warrington WA4 4AD

ISSN 0144-5677

Characteristics of TGM6

T.S.Turner and D.Teehan
SERC Daresbury Laboratory

February 1992

Contents

1. Introduction

Over the past 2 years several periods of commissiong time have been granted in order to characterise the performance of the Toroidal Grating Monochromator on station 6.2 of beam line 6 of the SRS. The purpose of this technical memorandum is to report the results within one document that can be used as a reference by in-house staff and users alike.

2. The Toroidal Grating Monochromator

The SRS produces a source of light whose dimensions are 2mm horizontally (FWHM) and 0.4mm vertically (FWHM) at the centre tangent of dipole magnet 6 (Mackay 1987).

The optical system (Figure 1.) for the station can be described as follows :

a. The white beam from the SRS (10mrad horizontal aperture) is horizontally deflected and focussed (at the entrance slit of the monochromator) by a cylindrical platinum coated SiC pre-mirror (M1). The object distance is 7m and the image distance is 3.5m. The angle of incidence is 70 degrees and the demagnification 2 : 1.

b. After M1 a second cylindrical platinum coated SiC pre-mirror (M2) is placed which deflects the beam vertically and focusses it at the entrance slits of the monochromator . The object distance is 8.4m and the image distance is 2.1m. The angle of incidence is 75 degrees and the demagnification is 4 : 1.

c. The light is monochromated by a toroidal, gold coated, lamellar, fused silica grating of either 710 l/mm or 1800 l/mm line density (G1 or G2). The entrance arm length is 1931mm (r) and the exit arm length is 3273mm (r_d). The grating included angle is 150 degrees (2θ) and the diffraction is in positive first order. G1 covers the photon energy range 15 - 60 eV ; G2 covers 40 - 140 eV.

The resolution achieved by the monochromator depends on several factors :

(i) The SRS electron beam size.

(ii) The vertical size of the photon beam at the entrance slit (S1).

(iii) The vertical size of the exit slit (S2).

(iv) The geometrical aberration limit of the monochromator.

(v) Residual geometrical/alignment errors.

d. The monochromatic image at the exit slit is then post-focussed by an ellipsoidal, gold coated, Spectrosil vertically deflecting mirror. The angle of incidence is 82.5 degrees and the demagnification 2 : 1. This provides a final spot size at the centre of the experimental chamber of < 2mm x 2mm and a photon flux of $> 10^{11}$ photons/second in a 0.3% bandpass (at 2GeV 100mA SRS). In order to make the beam incident on the sample in the horizontal plane a plane gold coated mirror is placed before the ellipsoid.

In addition to the energy resolution defining slits (Y1 and Y2) there are 4 pairs of jaws which can be brought in to block the path of the beam. These are coated with a phosphor and are used as an aid for alignment purposes and to restrict the beam if necessary. The following table describes the jaw positions :

JX1	Horizontally defining jaws near the focus of M1 and M2.
JX2	Horizontally defining jaws in front of the grating vessel.
JY1	Vertically defining jaws just in front of the grating vessel.
JX3	Horizontally defining jaws near the exit slit.

The grating monochromator works in the following way. Light of wavelength λ incident on the grating at angle α to the surface normal is either reflected (zero order) or diffracted at an angle β. The relative intensities of light with wavelength λ reflected or diffracted into a particular order k are determined by the groove shape and the dielectric constant. β is related to α, N the groove density and λ by the grating equation :

$$N k \lambda = \sin\alpha + \sin\beta \qquad (1)$$

α and β are of opposite sign if on opposite sides of the surface normal. Diffraction is possible over a range of incident and diffracted angles for a particular λ.

In the fixed deviation geometry :

$$\alpha - \beta = 2\theta \qquad (2)$$

Combining equations 1 and 2 :

$$\alpha = \sin^{-1}(N k \lambda / 2\cos\theta) + \theta \qquad (3)$$

$$\beta = \sin^{-1}(N k \lambda / 2\cos\theta) - \theta \qquad (4)$$

Rearrangement of equation 4 gives :

$$\lambda = (2 / N k)\cos\theta \sin(\theta+\beta) \qquad (5)$$

$(\theta+\beta)$ is the angle turned from zero order. λ is proportional to $\sin(\theta+\beta)$ and so a simple sine bar arrangement can be used to drive the monochromator. λ is then proportional to the perpendicular displacement L of the sine bar from the zero order position. L is measured using a commercial linear encoder.

The TGM6 monochromator operates with $k = +1$ i.e. in positive first order. A consequence of a fixed deviation geometry is that the long λ end of

the spectrum (low energy) is limited to the $\alpha = 90$ degrees case. Substituting for $\beta = \alpha - 2\theta$ in equation 5 the horizon limit λ_h is given by :

$$\lambda_h = (2 / N k)\cos^2\theta \qquad (6)$$

For TGM6 this gives horizon limits of 6.57eV and 16.65eV for G1 and G2 respectively.

For a comprehensive explanation of the theory of diffraction grating optics and other optical topics refer to West and Padmore (1986).

3. Radiation safety system

The beamline safety system was upgraded during the 1990/1991 winter shutdown. On 15th February 1991 the station was passed as radiation safe by the Health Physics group. The purpose of the system is to ensure that it is not possible to be exposed to radiation whilst a section of the station is up at air e.g. no parts of the body in the section which is not under vacuum. There is a set of vacuum switches (which operate at 200 mbar) controlling guard lines A and B on the control module for Valv01 (the radiation stop). This system is independent of the vacuum interlock system for controlling the opening and closing of beamline valves. If any of the vacuum switches show a fail condition then the mask (Mask A) and Valv01 will close. The safety switch system is routinely checked.

The radiation check included all viewports along the beamline and the straight through lead glass viewport at the rear of the experimental chamber (with zero order light illuminating it). The image on the rear window is a slight arc of approximate dimensions 17mm horizontally by 4mm vertically. A hand-held monitor is available on the beamline for anyone to check for radiation at any time.

The order in which to open the valves is as follows :

Valv03 - I_0 chamber / monochromator

Valv02 - monochromator / M2

Mask A - M1 / SRS

Valv01 - M2 / M1

Hence to illuminate the mirrors and grating all the beamline valves must be open. The experimental chamber must be under vacuum in order to satisfy the interlock for Valv03, but the manual valve between the chamber and the I_0 does not have to be open. This facilitates zero order calibration of the monochromator without exposing the sample to the beam.

4. Alignment of the optical system

When the beamline was constructed, the vacuum vessels and their internal components were surveyed into position using large scale metrology techniques. When necessary the survey procedure is repeated e.g. when components are removed for refurbishment and then replaced.

In order to operate the optical system correctly, several adjustments have to be made by users after light has hit the mirrors for the first time in an SRS fill. Once port 6 of the SRS is open, the beamline valves are opened as described above. This illuminates the pre-mirrors and allows them to warm up during steering of the SRS beam. Once user beam is established, the grazing angle of M1 is adjusted to bring the image central on JX2 with the micrometers typically set to 12mm. The adjustment device is a rotary drive, which projects out of the side of the line 6 mirror box, between the 6.2 line and the water cooled appendage to the mirror box. Adjustments of +/- 0.05 units are usual during a fill of the SRS (one full turn = 1 unit). JX2 should be reopened once M1 has been set. JX1 can also be used to check the

alignment, but because the entrance slit vessel has been removed quite often its usefulness as an absolute alignment aid (in the horizontal direction) is doubtful. The machine physicists sometimes make a change in the horizontal SRS orbit offset and the position of the beam on JX2 has to be judged accordingly by the station master. Currently a symmetric image is used but prior to this a delibrate offset to one side had been used compensating for the difference in the illuminated length of M1.

The movement across JX1 is around 10mm during the first hour or so depending on the magnitude of SRS beam current at the start of a fill. The beam continues to move during a fill and appears to be related to the decay of SRS beam current. For interest one night (August 1990) the mirrors were left exposed to light without continual correction of M1. User beam had been obtained at 20:15 at 185mA. M1 was adjusted so that, with JX2 set to 12mm, light was just visible on the left hand side (this was the setting used at that time for alignment). At JX2 the beam is about 35mm wide. The right hand jaw contained about 10mm of beam. At 08:50 the next morning the image on JX2 was such that only a small amount of light could be seen on the right hand side, with the left being exposed to around 10mm of beam i.e. the reverse of the profile of 12 hours earlier. The beam current was 131mA and the horizontal position had moved by around 10mm.

During an SRS fill the heat load on the pre-mirrors reduces. There is also a known SRS vertical beam drift with decreasing beam current (Quinn et. al. 1990). The monochromator is therefore operated with fairly wide open vertical entrance slits and M2 is not usually adjusted by users.

Once the entrance arm alignment is complete the lateral position of the grating must be checked. This is adjusted by turning a handle on the SRS side of the grating vessel. There are two grating positions marked on the drive ; 1 is the 710 l/mm grating, 2 is the 1800 l/mm grating. The monochromator needs to be close to zero order to carry out the rest of the alignment procedure. With JX3 set to 1mm on the micrometers the lateral position of the grating can be adjusted until the image is central on these jaws. JX3 need to be opened up for experimental use.

The zero order beam is then let into the experimental chamber in order to complete the alignment procedure. The internally mounted electron energy analyser has an aperture at the rear directly opposite the electron entrance apertures, allowing light to pass straight through the analyser. When the analyser is set to a polar angle of 180 degrees relative to the incident beam, the light is visible on the rear window of the chamber, provided the chamber is positioned correctly. Adjustment can be made to the chamber height and lateral position. Note that the image in the chamber is very sensitive to the alignment of the whole system and that the position of M1 has to be checked regularly. Fine tuning of the chamber position is carried out with monochromatic light and electrons emitted from the sample.

5. Zero order setting

To obtain photon energy calibration the monochromator must be set to zero order (see above). All grating positions are measured relative to the calibrated zero order position ($L = 0$). The grating is driven to the previous known position, where the beam is reflected ($\alpha = \beta$). The encoder on the sine bar lever arm reads 0.00. To compensate for changes in SRS vertical beam position and / or pre-mirror movements the grating angle is finely adjusted until the drain current measured from a tungsten grid beam monitor in the I_0 chamber is maximised and the encoder reset to 0.00.

In order that the zero order position for each grating be found correctly, measurements were made of the beam monitor output with encoder reading for each grating, without resetting the encoder zero between the two gratings. For 1mm of sine bar lever arm movement from zero the encoder reads -1.000. The results are shown in Figure 2. The important features to note are that the profile for both gratings is double peaked and that there is a difference in encoder units of about 0.060 between the two gratings. For each grating the larger of the two peaks must be selected. The difference between the two gratings may be expained by a slight difference in mechanical alignment within the mounts.

Typical zero order beam monitor drain currents are :

2.0×10^{-8} A - G1

6.0×10^{-8} A - G2

for an SRS current of 100mA and Y1 and Y2 = 5mm on the micrometers.

The zero order reference position is checked regularly - at least every SRS fill and every time a new grating is selected. A change in angle of incidence (α) is caused by any vertical beam movement. Since it is known that the SRS beam is prone to vertical beam movement and that pre-mirror warming may cause movement too then it is also usual to check the zero order reference several times during a fill. This is particularly important for users who require photon energy ($h\upsilon$) accuracy to better than 0.1 eV at 100 eV for example. During June 1990 the drift in zero order position was recorded over 5 fills of the SRS (Cafolla 1990). The time at which the encoder was initially zeroed was recorded and all susequent reset times during a fill. In between, the zero order position was recorded to monitor the drift. Figure 3 displays the data for one fill. It is clear that the drifts observed are significant and not easy to predict. Data for the other 4 fills do not show an identical pattern of drift, but are equally significant e.g. Figure 4 shows the data for the next fill. The error in $h\upsilon$ can be calculated by adding the zero order offset to L (sine bar lever arm displacement). For example, an offset of +0.04 mm in L gives an error in $h\upsilon$ of -0.14eV at a selected energy of 80eV i.e. the actual photon energy is 79.86eV. It is interesting to note that if zero order had not been recalibrated regularly then the error after 10 hours could have been +0.1 mm causing a calibration error of -0.36eV !

6. Flux output curves

The flux output for each grating has been measured on several occasions over the last 2 years. Photoemitted electrons from the 95% transmission tungsten grid beam monitor are measured by amplifying the drain current using a Keithley 427 current to voltage converter. A voltage to

frequency converter creates pulses that can be counted (1V = 10^6 counts/second). The amplifier gain was set to 10^9 V/A. The following conditions were applied :

(i) Y1 = 5mm. This corresponds to the entrance slits being almost 1mm open. A conversion between the micrometer reading and the actual slit opening allows for the gearing ratio of 2.39.

(ii) S2 was adjusted to provide a fixed contribution of 0.1eV at all hυ. Since aberrations and other factors also contribute to the resolution the output curve is not a genuine fixed energy resolution spectrum.

(iii) The data were normalised to 100mA SRS beam current.

Figures 5 and 6 show the results from February 1991. Note that the peak flux from G1 is roughly an order of magnitude higher than that from G2. These flux curves are typical and consistent with others measured over the last 2 years. No deterioration of the flux has occurred indicating that the optics have remained clean. Figure 7 shows flux curves measured at different times for G1. The slight differences may be explained by errors in setting of S2. In February 1991 the automatic exit slit operation was not working and so S2 was set by hand. The beam monitor used is permanently installed and has not been changed over the last 2 years.

Flux output curves have also been measured as drain current from a cleaned copper crystal placed in the experimental chamber . The V/I gain was 10^9 and conditions (i) - (iii) apply. The results are shown in Figures 8 and 9. The data agree to within a factor of 2 with similar data taken in March 1990. A difference in sample cleanliness is the most likely reason for this.

During one SRS fill the flux at 30eV was monitored as the beam current decayed. Over the range 200 - 160mA the output was approximately linear (see Figure 10).

7. Photon energy calibration

If hυ is changed by 5eV for example then the position of any feature in a photoemission spectrum should move by 5eV too. However, it is not unreasonable to expect a small calibration error across the hυ range of a grating, since it is unlikely that N is exactly 710 l/mm or 1800 l/mm. As has already been discussed above, SRS beam movements and mirror heating effects may affect calibration if zero order has not been checked. Any systematic error with the detection system must be taken into account e.g. errors in retarding potential set on the electron energy analyser. Each SRS dataset contains hυ, which is calculated from the actual lever arm position after it has been driven.

Consecutive Fermi edge spectra were taken within one hour of zero order calibration for each grating. The results are summarised in the following tables :

G1 (710 l/mm)	hυ (eV)	Excess shift in Fermi edge (eV)
	15.001	0.00
	17.999	0.00
	20.001	0.00
	24.999	0.01
	29.997	0.02
	35.003	0.02
	40.005	0.03
	45.002	0.06

G2 (1800 l/mm)	hυ (eV)	Excess shift in Fermi edge (eV)
	40.000	0.00
	50.001	0.01
	59.999	0.03
	69.991	0.02
	90.005	0.06
	99.993	0.1

Clearly, there appears to be a systematic shift in apparent photon energy for each grating e.g. at 40eV the actual hυ was 40.03eV on G1. These measured shifts are to be interpreted as a demonstration that there is an error. They are not intended to be an absolute calibration of the gratings. Users must take calibration scans (e.g. of the Fermi edge of a metallic part of the sample holder) before actual spectra are recorded if such errors are expected to be significant in their data analysis. Such data will reveal general calibration errors and any beam movement associated problems. The detector power supply was checked for systematic errors and none were found. i.e. no relative decrease in retarding voltage for increasing kinetic energies set was seen at a fixed pass energy.

8. Entrance and exit slit calibration

In order that S1 and S2 are set correctly the closed position (CP) needs to be known. For each slit CP can be found by monitoring the output of the beam monitor while closing the slit gradually, noting the micrometer reading. The CP for Y1 and Y2 have been measured and checked several times. For Y1, CP = 7.35mm ; for Y2, CP = 6.00mm. The slit conversion between the actual opening required (S) and micrometer reading (Y) is given by :

$$Y = CP - (2.39 \times S) \qquad (9)$$

The following table contains Y values for Y1 and Y2 for S values in the range 0.0 - 1.0mm.

S1(mm)	Y1(mm)	S2(mm)	Y2(mm)
0.0	7.35	0.0	6.00
0.1	7.11	0.1	5.76
0.2	6.87	0.2	5.52
0.3	6.63	0.3	5.28
0.4	6.39	0.4	5.04
0.5	6.16	0.5	4.81
0.6	5.92	0.6	4.57
0.7	5.68	0.7	4.33
0.8	5.44	0.8	4.09
0.9	5.20	0.9	3.85
1.0	4.96	1.0	3.61

9. Vertical beam movement across Y1(entrance slit)

Before the entrance arm beam monitor was fitted, the only monitor that could be used was the one in the I_0 chamber. Measurements were made of the I_0 output current with Y1 position for hυ = 40eV at subsequent times during a fill. The results of such a test are shown in Figure 11. The data show that the intensity rises slowly between slits closed and slits open during the first few hours of a fill, but that later on the output shows a much faster rise in signal. When the output rises most steeply, the beam is aligned centrally on the slits. Figure 11 shows that the beam has moved vertically with respect to the centre of the slits. This is why the monochromator cannot be operated with the entrance slits closed down. The magnitude of the movement is at least 0.2mm during the first few hours of a fill.

10. Second order content

Toroidal grating monochromators do not order sort. Significant diffraction efficiency at second order (k=2) may be expected. Using a program written by H.A.Padmore the diffraction efficiencies for each grating in first and second order have been calculated. The results are shown in Figures 12 and 13. In order to have an accurate idea of the expected second order flux at the experiment the reflectivities of the mirror surfaces must also be considered. It is very simple to get some idea of the second order effects by scanning over twice the kinetic energy range for $h\upsilon$ e.g. 0 - 40eV for $h\upsilon$ = 20eV. Such spectra have been recorded for $h\upsilon$ = 15, 20, 25, 30 and 35eV with G1, and $h\upsilon$ = 50, 60, 65 and 70eV with G2 using a tantalum polycrystalline sample. The peak heights of core levels and valence band features were measured in first and second order for each photoemission spectrum. The data were corrected using theoretical atomic cross-section data (Yeh and Lindau 1985), with some assumptions being made about the atomic nature of valence band features. The transmission function of the analyser with kinetic energy is not known and the data cannot therefore be used as an absolute measure of second order content. The ratio of second order to first order measured in the way described above is plotted in Figures 14 and 15. Clearly the second order effect is significant for both gratings. The fact that the relative percentage of second order appears to be higher at low $h\upsilon$ is probably due to the fact that the analyser is more efficient at low retarding ratios. Typically around 25% of the light is due to second order diffraction from the gratings. This fact must be considered very carefully when interpreting data. In the future it is hoped that some second order filters will be available with a reasonable transmission for the first order light (Quinn 1991).

11. Theoretical calculations of resolution

There are three contributory parts to the overall resolution achievable by a TGM type monochromator :

(i) The part set by the finite size of the beam at the entrance slit in the dispersive direction - $\Delta E1$

(ii) The part set by the finite size of the exit slit in the dispersive direction - $\Delta E2$

(iii) The geometrical aberration limit of the monochromator - $\Delta E3$

If the size of the images at entrance and exit slits are denoted by S1 and S2 respectively then the $\Delta\lambda$ contributions are :

$$\Delta\lambda_1 = (S_1 / N\,k\,r)\cos\alpha \qquad (7)$$

$$\Delta\lambda_2 = (S_2 / N\,k\,F)\cos\beta \qquad (8)$$

where r is the entrance slit to grating distance and F is the monochromatic image distance (West and Padmore 1986). Using the relation $E = hc/\lambda$, ΔE_1 and ΔE_2 are readily calculated. Using a program written by H.A.Padmore it is possible to calculate the geometrical aberration limit.

To calculate the overall resolution (Δ_{MONO}) the three contributions ΔE_1, ΔE_2 and ΔE_3 are added in quadrature. For G1 at $h\upsilon$ = 35eV with ΔE_2 selected to be 0.1eV :

$\Delta E_1 = 0.053$eV
$\Delta E_2 = 0.100$eV
$\Delta E_3 = 0.050$eV

giving Δ_{MONO} = 124meV. Note that this is significantly larger than the value selected for the exit slit and clearly shows the significance of the other contributions. The data acquisition software calculates the exit slit setting for a given user selected photon energy resolution but takes no account of the contributions ΔE_1 and ΔE_3.

The total experimental resolution is given by a combination of the monochromator resolution, Δ_{MONO}, the electron energy analyser resolution, ΔE_{ANAL}, and the inherent width of the feature being investigated. It is usual to operate the monochromator and analyser at similar resolution contributions, such that maximum signal is obtained at the required resolution. For instance, at room temperature the theoretical Fermi edge FWHM is 112meV (see equation 9). Thus, in order to measure this it would be sensible to select 25meV for each contribution. When added in quadrature this gives a 35meV instrumental contribution which is significantly smaller than the feature to be observed. In the valence band region of a spectrum typically peak widths are of the order 0.5eV and Δ_{MONO} and ΔE_{ANAL} are usually set to around 0.1eV each.

It is possible to calculate ΔE_1 and ΔE_2 for given slit sizes (S1 and S2 respectively) or the slit size needed to provide a required resolution contribution at a given photon energy. For ΔE_1, S1 is equal to the FWHM in the vertical direction of the image at the entrance slit, because the entrance slits are operated wide open for reasons discussed above. Using a beam monitor situated in the entrance arm of the monochromator S1 has been measured to be 0.35mm FWHM (white light). This value can be used as a worst case for S1 in the calculation. ΔE_1 calculated by this method is shown in Figures 16 and 17 for G1 and G2 respectively. For ΔE_2, it is more instructive to show S2 as a function of $h\upsilon$ at fixed ΔE_2. Figures 18 and 19 show exit slit size vs. $h\upsilon$ for $\Delta E_2 = 0.1$eV for G1 and G2 respectively.

A previous measurement of SRS source size shows a dependence on SRS beam current, with a vertical size of 0.4mm FWHM at 200mA (Haslam 1988). Using raytracing techniques it is expected that the size of the beam at the entrance slit would be 0.2mm FWHM in the vertical (H.A.Padmore 1990) with an SRS source size of 0.4mm FWHM. The measured value of 0.35mm clearly does not agree with the expected value. Pre-mirror aberrations caused by heat loading may be a contributory factor. During the 1991/1992 shutdown an improvement to the shielding of M1 is to be installed. Presently there is no direct cooling ; an indirectly cooled copper block is mounted near to the front edge of the mirror. However this block glows bright red if SRS beams are of the order 300mA and does not actually block the path of light to the front edge of the mirror. A larger block which has its own water supply is to be fitted.

Using the program written by H.A.Padmore, the geometrical aberration limit under the normal operating conditions of the instrument for G1 and G2 have been calculated. The results are shown in Figures 20 and 21. Each grating has a minimum in ΔE_3 for two photon energies. These correspond to the two $h\upsilon$ values for which the exit arm length (r_d) gives a zero defocus condition. r_d=3273mm has been selected to optimise the instrument over a reasonable range of energies for each grating. Defocus is the dominant aberration, with coma and astigmatic coma contributory factors. The parameters that these three terms depend on are :

(i) the entrance arm length, r

(ii) the exit arm length, r_d

(iii) the TGM included angle, 2θ

(iv) the toroidal grating sagittal and meridian radii

(v) the illuminated area of the grating surface

The details of the theory behind the calculation of ΔE_3 are in West and Padmore (1986). In principle it is possible to adjust r_d and the grating masks to select a given operating resolution for a particular $h\upsilon$. Adjustment of r_d is only suitable for the energy chosen and may affect other energies in a more dramatic way.

12. Electron energy analyser characterisation

In August 1990 the energy resolution capability of the in-situ VG ADES quasi-hemispherical analyser was investigated. There are two other analysers that can be installed on the station; the Perkin Elmer CMA (cylindrical mirror analyser) and the VSW HA100 (hemisperical analyser). However these have not been used in any characterisation experiments by us. The photon source used was a helium discharge lamp which provides photons of energy 21.2eV at a linewidth of less than 5meV. Tantalum Fermi edge spectra were recorded at a sample temperature of approximately 20K using a liquid helium cooled manipulator (Teehan 1991). The raw spectra were smoothed and differentiated in order that a FWHM measurement be made. If a theoretical Fermi function is considered :

$$f = 1/(e^{(\varepsilon - \mu)/k_b T} + 1) \qquad (9)$$

the 15% - 85% width corresponds to the FWHM. The FWHM analyser resolution function ΔE_{ANAL} is given approximately by :

$$\Delta E_{ANAL} / E_{pass} = d / 2r_0 + \alpha^2_{max} \qquad (10)$$

where E_{pass} is the analyser pass energy, d is the exit aperture dimension in the energy dispersive direction, r_0 is the mean radius of the hemispheres and α_{max} is the limiting pencil angle in radians.

The experimental results are summarised as follows :

Pass energy eV	Measured FWHM meV	Fermi edge position eV	Theoretical FWHM meV	Intensity c/s
2	73	16.84	22	250
5	81	16.81	54	650
10	86	16.74	108	1000
20	191	16.61	216	2250

The contribution to the measured FWHM from the inherent Fermi edge width is 12meV at T = 20K, which when deconvolved from the measured FWHM does not affect the result significantly. Hence the measured FWHM can be taken as a measure of the analyser resolution. The results are plotted out in Figures 22 to 24. The resolution does not improve significantly at pass energies below 10eV. The achievable resolution of 86meV is adequate for most user experiments. The 1mm analyser entrance aperture was fitted. There is a consistent change of apparent feature position with pass energy. This is probably due to a systematic setting error in the analyser power supply. This behaviour is reproducible but care must be taken with the analysis of data if more than one pass energy is used for an experiment. The rapid reduction in analyser transmission at 2eV pass energy is probably due to stray fields. Other apertures are available for the analyser so that the angular acceptance can be changed. However when a 0.5mm aperture is fitted the intensity vs. E_{pass} performance is inferior (Turner 1990).

13. Measured resolution of the monochromator

13.1 710 l/mm grating

An example of one of the narrowest Fermi edge widths observed is shown in Figure 25 ; $h\upsilon$ = 18eV, E_{pass} = 5eV, ΔE_2 = 0.05eV, Y1 = 5mm and T ~ 20K. The FWHM is 71meV +/- 10meV.

Several spectra have been measured over the last 2 years in order to determine the performance of the monochromator. All data were measured under the following conditions :

(i) r = 1931mm

(ii) r_d = 3273mm

(iii) E_{pass} = 5eV

(iv) Sample temperature ~ 20K

(v) Y1 = 5mm

(vi) $\Delta E_2 = 50meV$

It is possible to calculate the Δ_{MONO} contribution for each photon energy using the above parameters and the following assumptions :

(i) R = 10m (meridian radius of the grating)

(ii) $\rho = 0.628m$ (sagittal radius of the grating)

(iii) the whole of the grating is exposed to light (100mm x 40mm)

Δ_{MONO} for S1 = 0.35mm is shown in Figure 26. The trend for Δ_{MONO} is to increase with hυ, due to the contribution of ΔE_1 . ΔE_2 is a fixed contribution of 50meV. ΔE_3 has some structure to it, in particular two dips which correspond to the two in focus positions at $r_d = 3273mm$.

The overall expected resolution has to take into account the analyser contribution ΔE_{ANAL}. Figure 27 shows the measured FWHM vs. hυ, the measured FWHM being a convolution of ΔE_{ANAL} and measured Δ_{MONO}. The error bar for each measurement is +/- 10meV. The plot also shows the expected FWHM using a ΔE_{ANAL} of 70meV. This is an educated guess for ΔE_{ANAL}. The measurements made in August 1990 would imply that a value of 81meV should be used but this cannot be correct because Fermi edge widths of 80meV have been measured, which would eliminate Δ_{MONO}. The agreement at low photon energies is quite good but as hυ increases the difference becomes large. At low hυ the dominant contribution to Δ_{MONO} is ΔE_2 . At higher hυ the major contributor is ΔE_3. This is critically dependent on the physical geometry of the grating and the alignment of the whole

instrument. Hence from the results it may be reasonable to conclude that alignment error or grating manufacturing errors are to blame for the poorer performance at higher hυ values.

A fit of the measured values of resolution to a set of calculated "expected" data has been made by a recalculation of Δ_{MONO} assuming that the focus of the pre-mirror system is 31mm closer to the gratings. A dramatic change in the behaviour of ΔE_3 is seen. Astigmatic coma, defocus and coma are all affected by a change in r. Figure 28 shows the "expected" and measured values of resolution. The values used for ΔE_1 were not changed from those previously calculated using an S1 value of 0.35mm and r=1931mm. A slight change to S1 may be expected, but since the change in r of 31mm is not very large it is reasonable to expect that S1 will not change dramatically. Similarly the change in r introduces only a small scaling factor into the equation for $\Delta\lambda_1$ (see equation 7). The purpose of this exercise is to investigate any dominating effects. The agreement between the "expected" and the measured data is much better than that in Figure 27. A likely explanation for an apparent change in r is that the focussing of M1 and M2 depends on the radii of the mirrors and the exact position of the tangent point relative to the position of M1.

Adjustment of the exit arm length changes the defocus aberration. The distance between the gratings and the exit slit is easily measured and is 3273mm +/- 2mm. Changing the sagittal radius of the grating affects only the astigmatic coma contribution. Changing ρ by 20% in the calculation of ΔE_3 had no significant effect. Changes in the meridian radius did not provide a satisfactory match of measured to "expected" data.

In summary, it is likely that there is a focussing error in the pre-optics which gives a change in effective entrance arm length and that grating G1 has been manufactured close to the specified radii.

13.2 1800 l/mm grating

Spectra have been measured under the following conditions :

(i) r = 1931mm

(ii) r_d = 3273mm

(iii) E_{pass} = 10eV

(iv) Sample temperature ~ 20K

(v) Y1 = 5mm

(vi) ΔE_2 = 100meV

Δ_{MONO} for S1 = 0.35mm is shown in Figure 29. The calculation assumed the same conditions as for G1. Again the trend for Δ_{MONO} is to increase with hυ. At low photon energies the contribution of ΔE_2 is significant, but as hυ increases the contributions of ΔE_1 and ΔE_3 increase such that they contribute almost equally at hυ = 85eV. At higher energies ΔE_3 is most significant.

The measured FWHM are shown in Figure 30 along with the expected values calculated assuming a ΔE_{ANAL} contribution of 86meV. Again the agreement between expected and measured values is poor, particularly as the photon energy increases. An attempt has been made to fit the measured data to set of "expected" data. In order to be consistent with the analysis of G1 an entrance arm length of 1900mm has been used in calculation of ΔE_3. A reasonable fit is obtained for a meridian radius of 9.8m, which corresponds to a manufacturing error of 2% (Figure 31). This corresponds to a large defocus error, which could be corrected by adjustment of the exit slit position. Recalculation of the errors at the new r_d would have to be done to predict the behaviour of Δ_{MONO} across the photon energy range.

13.3 Alignment of the beam at JX2 (grating mask)

A test was carried out to determine whether the achievable resolution is dependent on the beam alignment at JX2. This can be considered as a similar test to the adjustment of the grating yaw since the in-plane angle of incidence is changing. Photon energies of 18 and 30 eV were used. Fermi edge spectra of cooled tantalum were taken with the light aligned to the left, in the centre and to the right on JX2. The conditions listed above for G1 were used. The results are summarised as follows :

hυ (eV)	FWHM (meV)	LHS or RHS filled
18	72	RHS
18	78	LHS
18	84	EVEN
30	135	RHS
30	135	LHS
30	136	EVEN

Within the error bar of measurement (+/- 10meV) the different alignment positions do not give rise to a change in performance.

13.4 Closing down the entrance slit

To determine the relative effect of beam size at the entrance slit the Fermi edge width of tantalum was measured but with the entrance slit closed such that Y1 = 7mm. This corresponds to a beam size at Y1 of 0.15mm. Using the entrance arm beam monitor the signal was maximised by adjusting the angle of pre-mirror M2. Data were taken over the energy range 18 - 40eV. Figure 31 shows the results along with those obtained under normal conditions (Y1 = 5mm). No significant differences are observed. This result adds weight to the analysis of the measured resolution data which

show that errors in ΔE_3 dominate and any expected changes in ΔE_1 due to a change in S1 are not observable experimentally.

14. Polarisation

The polarisation characteristic of TGM6 has been measured prior to the installation of the post-focussing mirror by D.S-L.Law, H.A.Padmore and F.M.Quinn in 1986. The method used was that of Rabinovich et. al. (1965). The method consists of taking two measurements of the reflectance of a mirror at 45 degrees angle of incidence : one with the plane of incidence perpendicular to the exit slit of the monochromator, R_1, the other parallel to the slit, R_2. The degree of plane polarisation, P, is given by :

$$P = (R_2-R_1) / (1+R_1+R_2-(1+4(R_1+R_2))) \qquad (11)$$

where $R_1=I_1/I_0$ and $R_2=I_2/I_0$. I_0 is the incident beam intensity and $I_{1,2}$ are the reflected intensities. The data show a decrease in P from around 70% to 40% over the photon energy range of 15 - 80eV. Calculations for the polarisation derived from the output of the storage ring (pre-HBL), the angular acceptance of the monochromator, and the difference in s and p reflectivities of the optical elements gives :

$P (h\upsilon = 20eV) = 79.6\%$
$P (h\upsilon = 45eV) = 61.9\%$
$P (h\upsilon = 75eV) = 58.6\%$

Clearly the trend in measured P with $h\upsilon$ is consistent with that calculated. It is hoped that an up-to-date measurement of P will be carried out during 1992.

15. Possible future improvements

a. Pre-mirror M1 has no direct cooling at present. Improvements to the indirect cooling will be done in the long 1991/1992 shutdown.

b. Second order filters will be bought in 1992.

c. If the entrance slit vessel were translatable up and down the entrance arm then it would be possible to investigate whether the slits were actually at the correct focus of the pre-optics.

d. The vertical beam movement at the entrance slit could be controlled if the angular adjustment of M2 were motorised along with Y1, and linked to the entrance arm beam monitor. This may prove very difficult because of the backlash in the M2 mechanism.

e. The resolution of G2 with varying exit slit position along the beamline needs to be measured at a fixed $h\upsilon$.

f. The radii and general geometry of the gratings could be measured. This has to be considered carefully because of the potential for grating damage if removed and the time required to recommission the monochromator when returned. This may help to decide whether any alignment errors are significant. Nothing can be done about any grating manufacturing imperfections but alignment can be corrected and r_d can be adjusted for G2 if necessary.

g. The shared mirror box in which M1 is mounted could do with a sturdier frame. The current support is not particularly rigid. This type of improvement may improve stability.

16. Summary

The performance of the SRS line 6 Toroidal Grating Monochromator has been measured and reported . The flux output is high enough for the majority of users and is reproducible from year to year. There appears to have been no degradation in performance in terms of flux. However, the achievable resolution has not been as good as was hoped. At the optimum $h\upsilon$ for G1 (18eV - corresponding to the zero defocus condition) the achievable

resolution is quite good. However, at non-ideal hυ values the resolution is not so good. For G2 the agreement is poor and becomes increasingly so with increased hυ. Alignment and/or geometrical errors are the likely cause of imperfect resolution performance. The system is characterised now and users have a reasonable idea of what to expect.

17. Acknowledgements

We would like to thank H.A.Padmore and F.M.Quinn for helpful discussions and D.Norman for his encouragement.

Appendix 1

Benchmarks

a. 710 l/mm grating flux output.

Measurement conditions :

(i) $Y1 = 5mm$
(ii) $\Delta E_2 = 0.1eV$
(iii) $h\upsilon = 10 - 100eV$
(iv) signal is drain current measured from a 95% transmission W grid permanently installed beam monitor, set up so that the signal is actually minimised i.e. the solid frame which supports the grid does not interfere with the monochromatic beam
(v) signal normalised to 100mA SRS beam current

Expected values :

$h\upsilon = 18eV \quad 1.5 \times 10^{-10}$ A
$h\upsilon = 30eV \quad 3.5 \times 10^{-10}$ A
$h\upsilon = 40eV \quad 2.0 \times 10^{-10}$ A

For a clean copper sample at the focus the drain current at 30eV has been measured to be 1.6×10^{-9} A ; this is equivalent to 2.0×10^{11} photons per second in a 0.1eV band pass at 100mA SRS beam current (assuming a photoelectric yield of 5%).

The signal measured on the beam monitor in zero order with Y1 = 5mm is expected to be 3×10^{-8}A normalised to 100mA.

b. 1800 l/mm grating flux output.

Measurement conditions :

(i) Y1 = 5mm
(ii) ΔE_2 = 0.1eV
(iii) hυ = 40 - 150eV
(iv) signal is drain current measured from a 95% transmission W grid permanently installed beam monitor, set up so that the signal is actually minimised i.e. the solid frame which supports the grid does not interfere with the monochromatic beam
(v) signal normalised to 100mA SRS beam current

Expected values :

hυ = 45eV - 5.7×10^{-11} A
hυ = 60eV - 6.0×10^{-11} A
hυ = 80eV - 5.0×10^{-11} A
hυ = 100eV - 3.0×10^{-11} A

For a clean copper sample at the focus the drain current at 90eV has been measured to be 6.5×10^{-10} A ; this is equivalent to 5.0×10^{10} photons per second in a 0.1eV band pass at 100mA SRS beam current (assuming a photoelectric yield of 5%).

The signal measured on the beam monitor in zero order with Y1 = 5mm is expected to be 6×10^{-8}A normalised to 100mA.

Note that flux output checks can be made by users at any time.

c. 710 l/mm resolution check.

Measurement conditions :

(i) FWHM Fermi edge width of Ta cooled to ~ 20K using a UHV compatible cryostat
(ii) Electron energy analyser pass energy set to 5eV
(iii) Y1 = 5mm
(iv) ΔE_2 = 50meV

Expected values :

hυ = 18eV 80meV +/- 10meV
hυ = 30eV 140meV +/- 10meV

d. 1800 l/mm resolution check.

Measurement conditions :

(i) FWHM Fermi edge width of Ta cooled to ~ 20K using a UHV compatible cryostat
(ii) Electron energy analyser pass energy set to 10eV
(iii) Y1 = 5mm
(iv) ΔE_2 = 100meV

Expected values :

hυ = 45eV 170meV +/- 25meV
hυ = 70eV 240meV +/- 25meV

e. Spot size.

The spot size at the sample has been measured by D.Law in 1988 to be 1mm x 1mm (+/- 0.1mm) FWHM between $h\upsilon$ = 20eV and 50eV using G1. With G2 the vertical dimension is 1mm (+/- 0.1mm) FWHM but the horizontal dimension is 2mm (+/- 0.1mm)FWHM over the range 50 to 105eV.

References

A.A.Cafolla - Team leader Cardiff user group, personal communication (1990)

S.M.Haslam - Daresbury SRS/APES/88/28 (1988)

H.A.Padmore - personal communication (1990)

F.M.Quinn - personal communication (1991)

P.D.Quinn, J.N.Corlett, M.W.Poole and S.L.Thomson - European Particle Accelerator Conference No. 2 (1990) Vol. 1 134 Editions Frontieres and DL Preprint DL/SCI/P699E (1990)

K.Rabinovitch, L.R.Canfield and R.P.Madden - Applied Optics 4 (8) (1965) 1005

D.Teehan - Daresbury Laboratory Technical Memorandum DL/SCI/TM82E 1991

T.S.Turner - TGM6 Technical Information Letter (1 January 1990)

J.B.West and H.A.Padmore - Daresbury Preprint DL/SCI/P536E (1986) and Synchrotron Radiation Handbook Volume 2 (1987) Amsterdam: North Holland

J.J.Yeh and I.Lindau - Atomic Data and Nuclear Data Tables 32 (1985) 1

Figure Titles

Figure 1. Layout of TGM on beamline 6.

Figure 2. Zero order profiles G1 and G2.
Beam monitor drain current measured as a function of lever arm displacement for both gratings around zero order. Signal normalised to 100mA SRS beam current. Note that the encoder zero was not reset between the two sets of measurements.

Figure 3. Zero order offset at t~1hr after reset.
Lever arm offset at 1 hour after re-establishing zero order several times during an SRS fill.

Figure 4. Zero order offset at t~1hr after reset : Next fill.
Lever arm offset at 1 hour after re-establishing zero order several times during the SRS fill after that shown in Figure 3.

Figure 5. Flux output, G1 : February 1991.
Beam monitor drain current as a function of photon energy, normalised to 100mA SRS beam current, 710 l/mm. Exit slit size varied with photon energy to provide a resolution contribution of 0.1eV.

Figure 6. Flux output, G2 : February 1991
Beam monitor drain current as a function of photon energy, normalised to 100mA SRS beam current, 1800 l/mm. Exit slit size varied with photon energy to provide a resolution contribution of 0.1eV.

Figure 7. Flux output, G1 : August 1990, Febuary 1991.
Conditions as for Figure 5.

Figure 8. Flux output, Cu, G1 : February 1991.
Drain current from copper as a function of photon energy, normalised to 100mA SRS beam current, 710 l/mm. Exit slit size varied with photon energy to provide a resolution contribution of 0.1eV.

Figure 9. Flux output, Cu, G2 : February 1991.
Drain current from copper as a function of photon energy, normalised to 100mA SRS beam current, 1800 l/mm. Exit slit size varied with photon energy to provide a resolution contribution of 0.1eV.

Figure 10. 30eV photon flux vs. SRS beam current.
Beam monitor drain current at 30eV photon energy at four times during an SRS fill, 710 l/mm. Exit slit set for a resolution contribution of 0.1eV.

Figure 11. I_0 vs. Y1 micrometer after increasing exposure to beam.
Beam monitor drain current as a function of Y1 micrometer reading at 1,2,3 and 5 hours of exposure of pre-mirrors to beam. Photon energy selected = 40eV (710 l/mm).

Figure 12. G1 : k = 1,2 diffraction efficiency.
Calculated first and second order diffraction efficiencies , 2θ=150 degrees, groove depth = 395 Angstroms, groove width = 8000 Angstroms, 710 l/mm.

Figure 13. G2 : k = 1,2 diffraction efficiency.
Calculated first and second order diffraction efficiencies , 2θ =150 degrees, groove depth = 180 Angstroms, groove width = 3200 Angstroms, 1800 l/mm.

Figure 14. G1 measured second order content.
Content estimated by dividing the second order peak height of a tantalum feature by the first, with corrections being made for atomic cross-sections (valence band features assumed to be 5d like). Note no correction for analyser transmission function with kinetic energy has been made. Errors bars show experimental statistical error only. 710 l/mm.

Figure 15. G2 measured second order content.
Content estimated by dividing the second order peak height of a tantalum feature by the first, with corrections being made for atomic cross-sections (4f core levels). Note no correction for analyser transmission function with kinetic energy has been made. Errors bars show experimental statistical error only.
1800 l/mm.

Figure 16. Calculated entrance slit size contribution for S1=0.35mm : G1.
Resolution contribution (ΔE_1) for a beam size of 0.35mm FWHM at the entrance slit, 710 l/mm.

Figure 17. Calculated entrance slit size contribution for S1=0.35mm : G2.
Resolution contribution (ΔE_1) for a beam size of 0.35mm FWHM at the entrance slit, 1800 l/mm.

Figure 18. Exit slit size for 0.1eV contribution, G1.
S2 in mm for $\Delta E_2 = 0.1$eV. 710 l/mm.

Figure 19. Exit slit size for 0.1eV contribution, G2.
S2 in mm for $\Delta E_2 = 0.1$eV. 1800 l/mm.

Figure 20. Calculated geometrical aberration contribution, G1.
710 l/mm theoretical limit (ΔE_3) under the following conditions:
(a) entrance arm length = 1931mm.
(b) exit arm length = 3273mm.
(c) grating included angle $2\theta = 150$ degrees.
(d) sagittal radius of grating = 0.628m.
(e) meridean radius of grating = 10m.
(f) whole of grating illuminated.
The three aberrations used in the calculation are defocus, astigmatic coma and coma.

Figure 21. Calculated geometrical aberration contribution, G2.
1800 l/mm theoretical limit (ΔE_3) under the following conditions :
(a) entrance arm length = 1931mm.
(b) exit arm length = 3273mm.
(c) grating included angle $2\theta = 150$ degrees.
(d) sagittal radius of grating = 0.628m.
(e) meridean radius of grating = 10m.
(f) whole of grating illuminated.
The three aberrations used in the calculation are defocus, astigmatic coma and coma.

Figure 22. Measured and theoretical analyser resolution.
Variation of resolution with analyser pass energy.
Measured data are FWHM Fermi edges of tantalum at 20K, He I discharge source. Theoretical values calculated using equation 10.

Figure 23. Intensity vs. analyser pass energy.
Measured signal at the top of the Fermi edge as a function of analyser pass energy.

Figure 24. Fermi edge position vs. pass energy.
The data show a systematic error with pass energy attributable to a setting error in the analyser power supply.

Figure 25. Tantalum Fermi edge, 18eV photon energy, raw data.
One of the narrowest Fermi edge widths observed (71 meV +/- 10meV). Sample temperature ~ 20K, analyser pass energy 5eV, Y1 = 5mm, $\Delta E_2 = 50$meV, 710 l/mm.

Figure 26. Calculated monochromator contribution, G1.
Combination of entrance slit, exit slit (50meV fixed contribution) and geometrical aberration contributions, as a function of photon energy, 710 l/mm.

Figure 27. Measured and expected FWHM, G1.
Measured FWHM Fermi edge width of cooled tantalum at 20K, analyser pass energy 5eV, Y1 = 5mm, ΔE_2 = 50meV, 710 l/mm. Expected values are the quadrature sum of Δ_{MONO} in Figure 26 and Δ_{ANAL} = 70meV.

Figure 28. Measured and "expected" FWHM, G1 (r = 1.9m).
Measured as in Figure 27. Expected values are quadrature sum of Δ_{MONO} (calculated with entrance arm length = 1.9m) and Δ_{ANAL} = 70meV.

Figure 29. Calculated monochromator contribution, G2.
Combination of entrance slit, exit slit (100meV fixed contribution) and geometrical aberration contributions, as a function of photon energy, 1800 l/mm.

Figure 30. Measured and expected FWHM, G2.
Measured FWHM Fermi edge width of cooled tantalum at 20K, analyser pass energy 10eV, Y1 = 5mm, ΔE_2 = 100meV, 1800 l/mm. Expected values are the quadrature sum of Δ_{MONO} in Figure 29 and Δ_{ANAL} = 86meV.

Figure 31. Measured and "expected" FWHM, G2 (r = 1.9m, R = 9.8m).
Measured as in Figure 30. Expected values are quadrature sum of Δ_{MONO} (calculated with entrance arm length = 1.9m and meridian radius = 9.8m) and Δ_{ANAL} = 86meV.

Figure 32. Measured FWHM, Y1 = 5mm and 7mm.
Comparison between source size limited case (Y1 = 5mm) and entrance slit size set to 0.15mm (Y1 = 7mm).
Tantalum sample at 20K, analyser pass energy 5eV, ΔE_2 = 50meV, 710 l/mm.

Figure 1.
Layout of TGM on beamline 6.

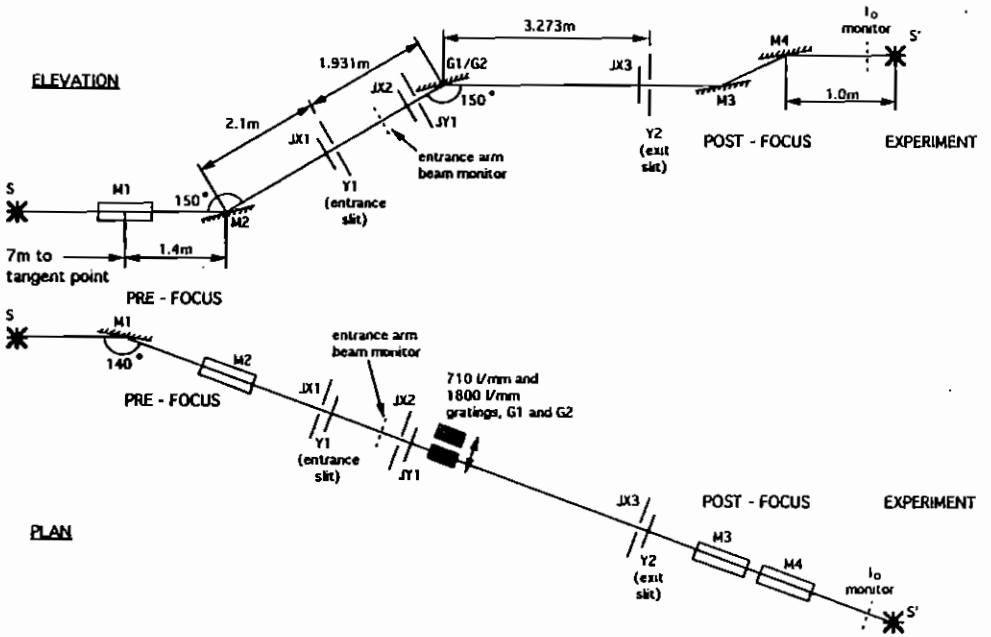

Figure 2.

Zero order profiles, G1 and G2.

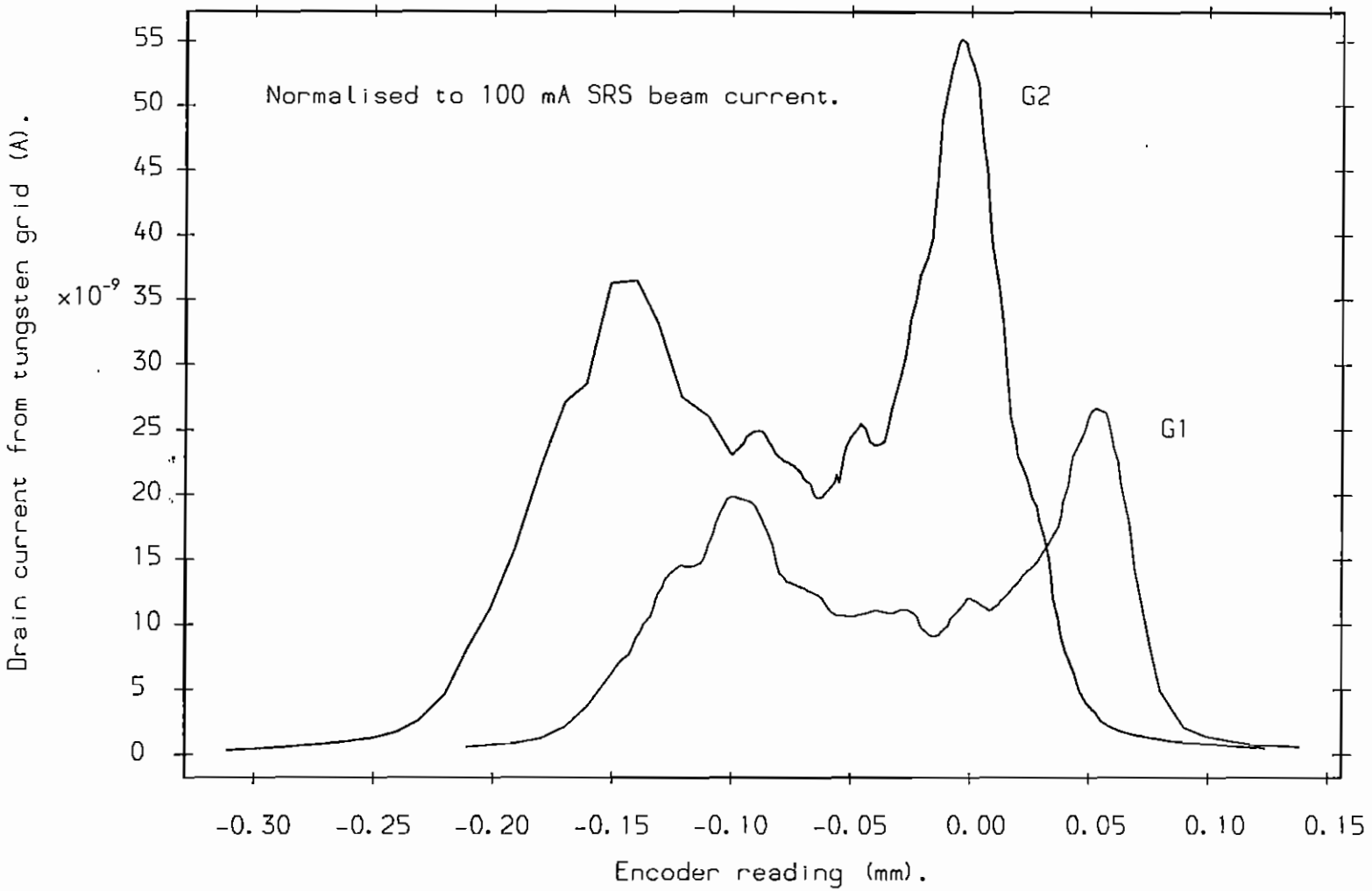

Figure 3.
Zero order offset at t ~1hr after reset.

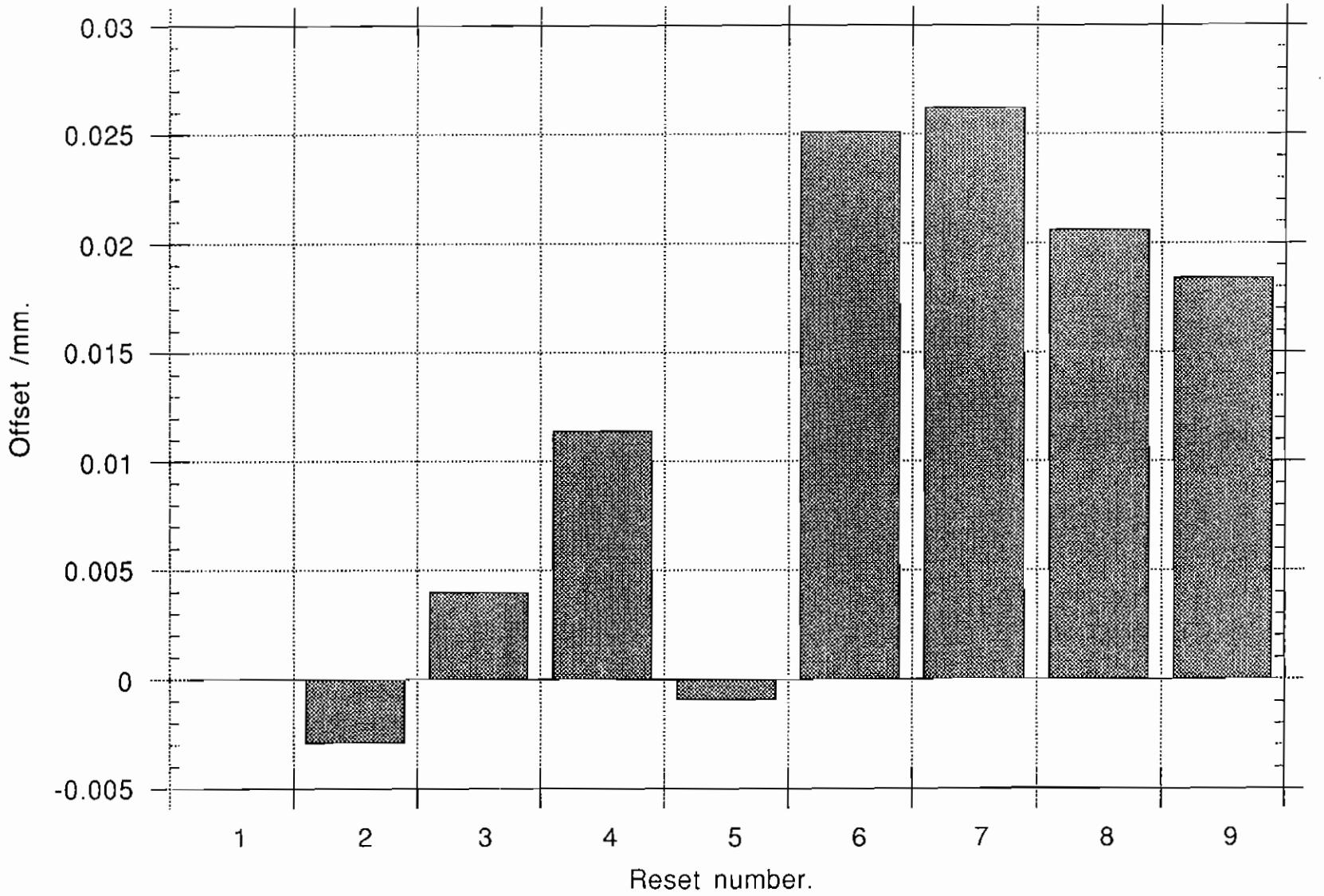

Figure 4.
Zero order offset at t ~1hr after reset: next fill.

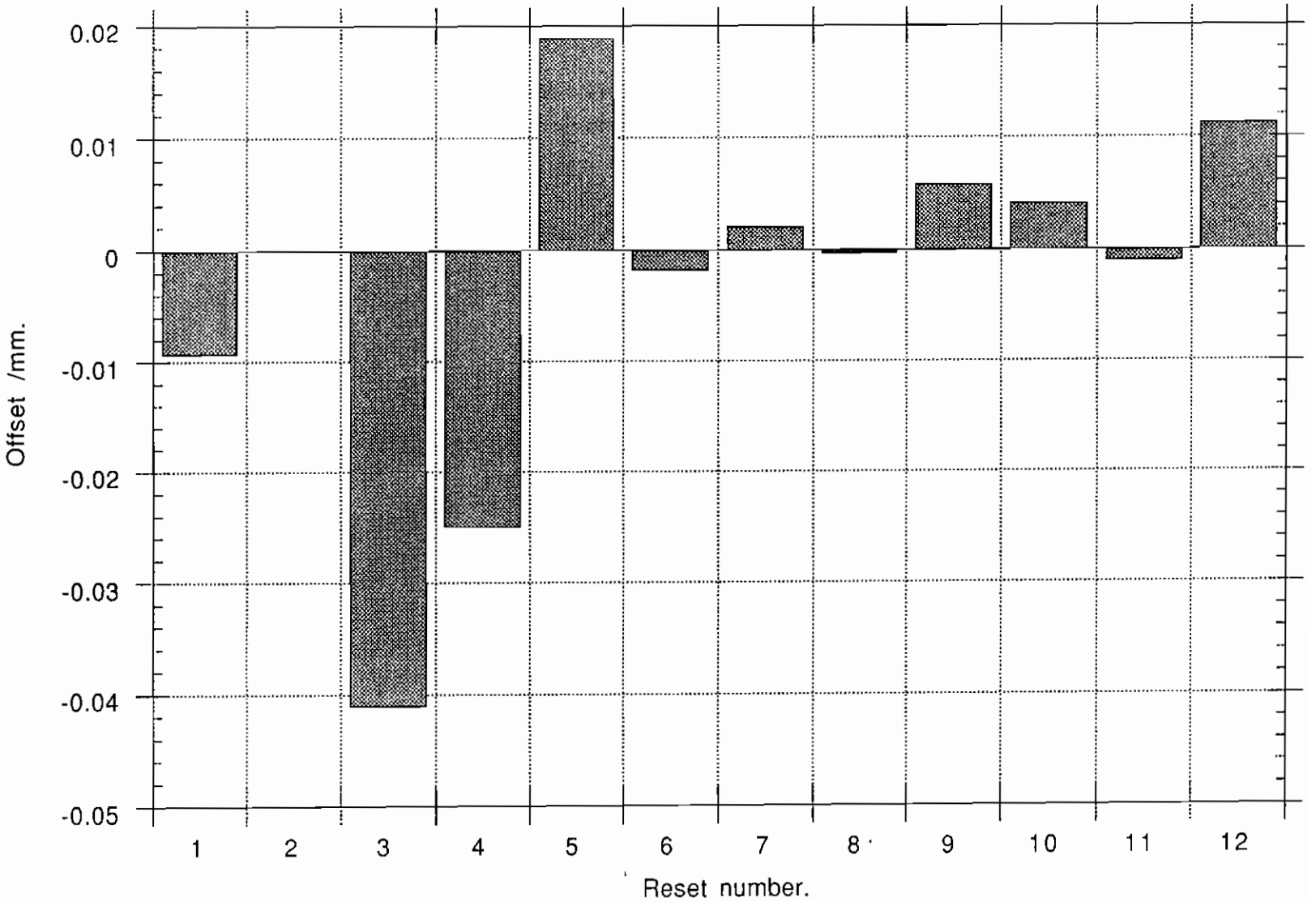

Figure 5.

Flux output, G1: February 1991.

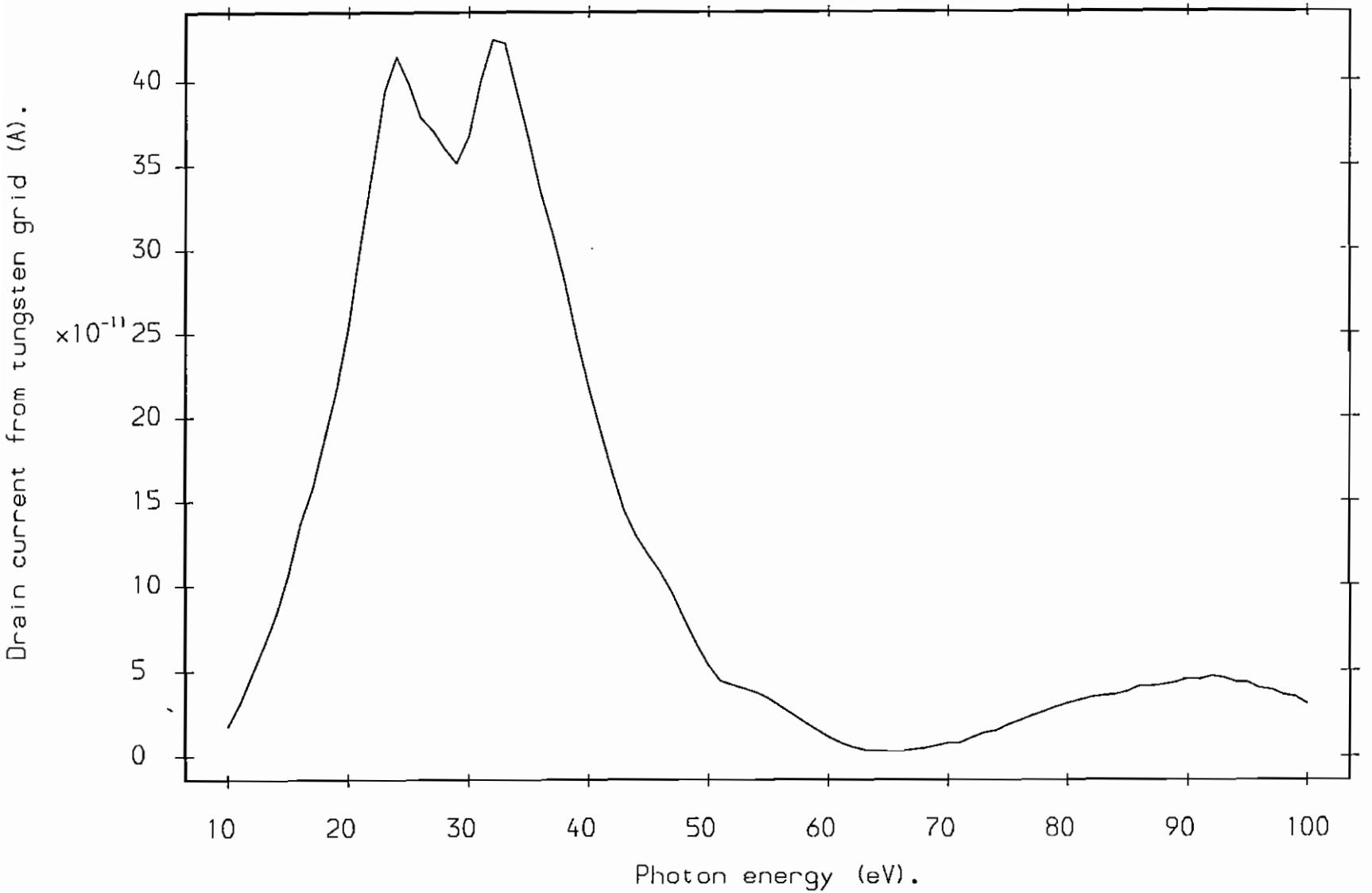

Figure 6.

Flux output, G2: February 1991.

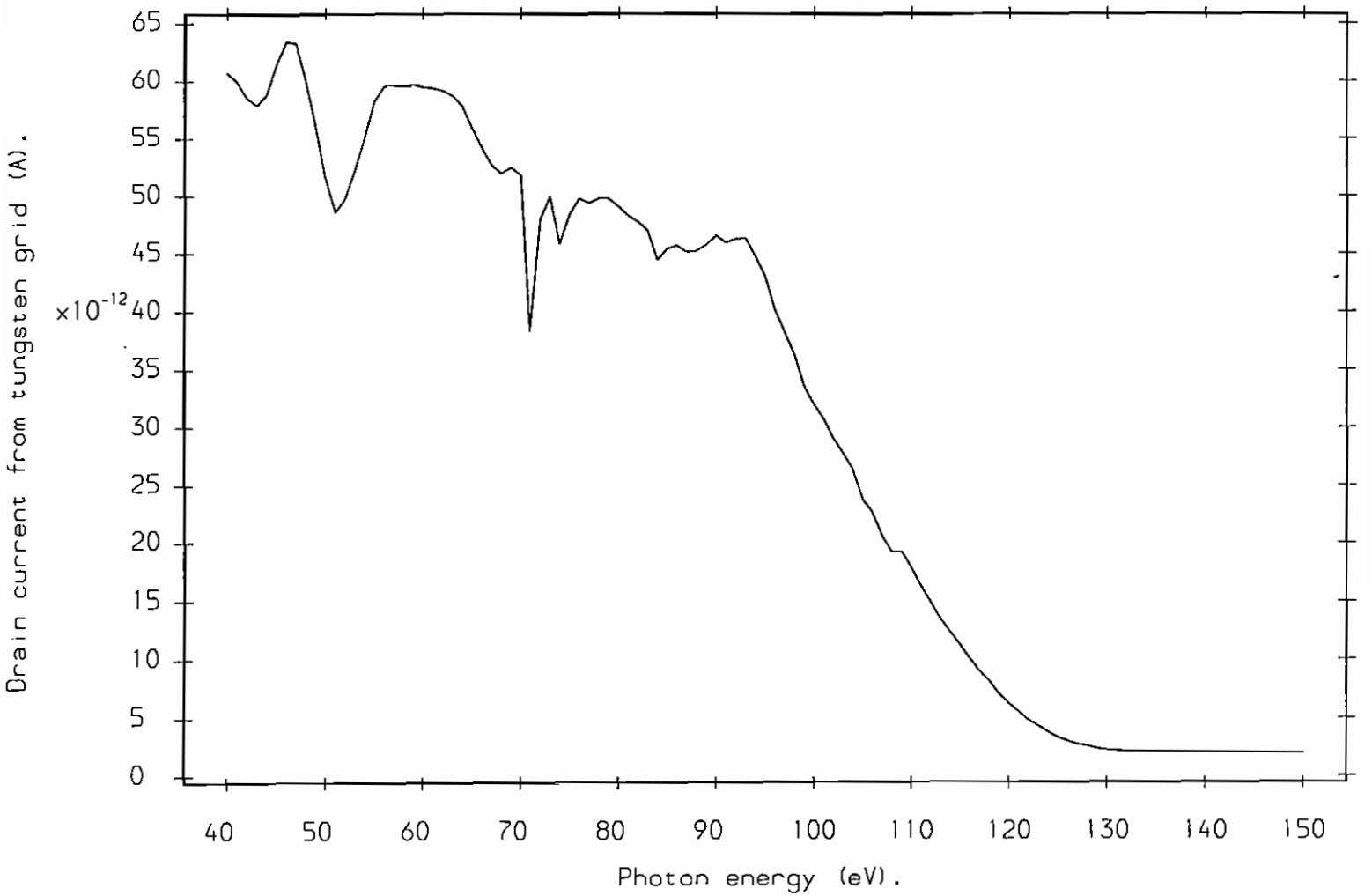

Figure 7.

Flux output, G1: August 1990, February 1991.

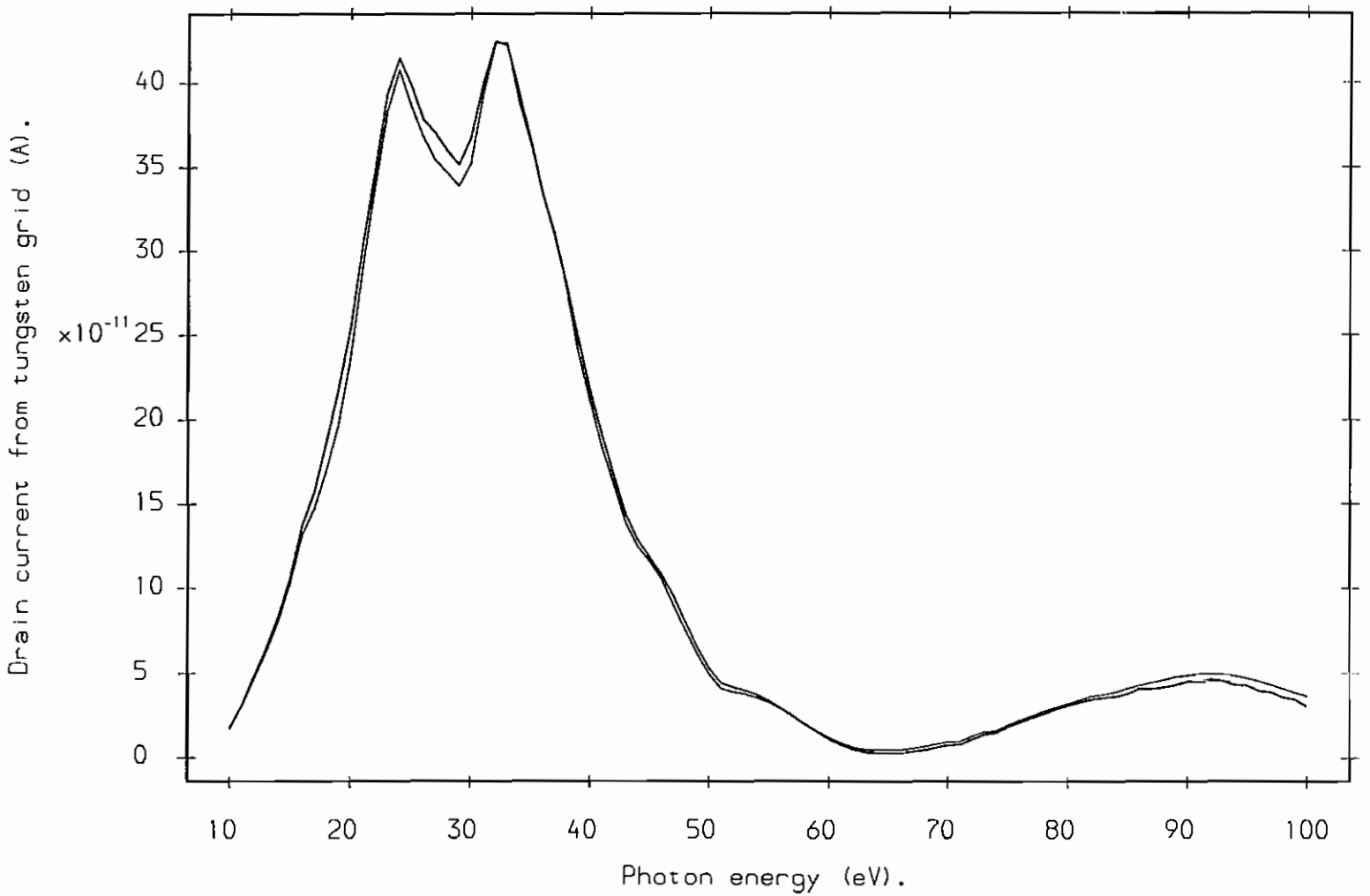

Figure 8.

Flux output, Cu, G1: February 1991.

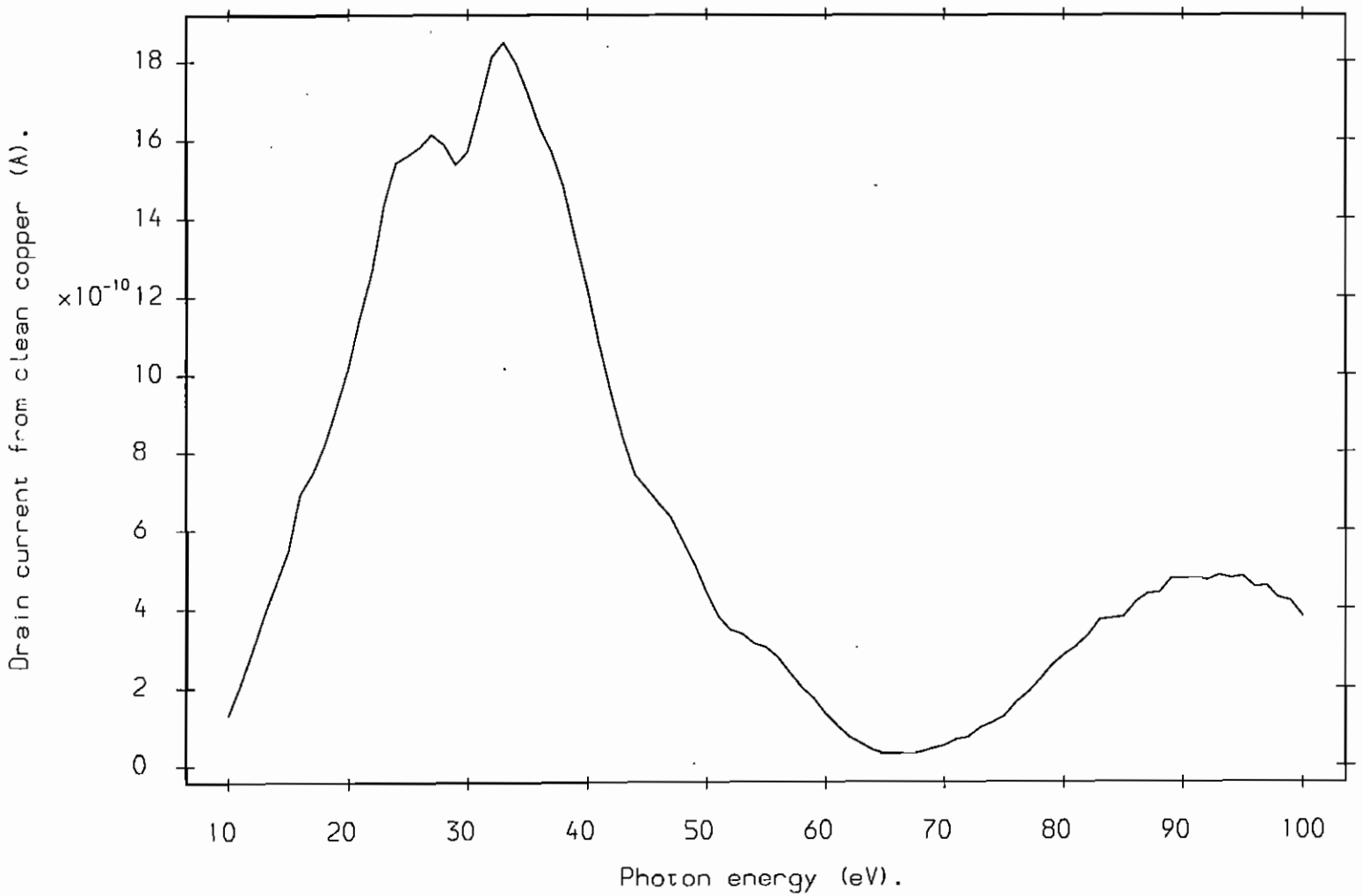

Figure 9.

Flux output, Cu, G2: February 1991.

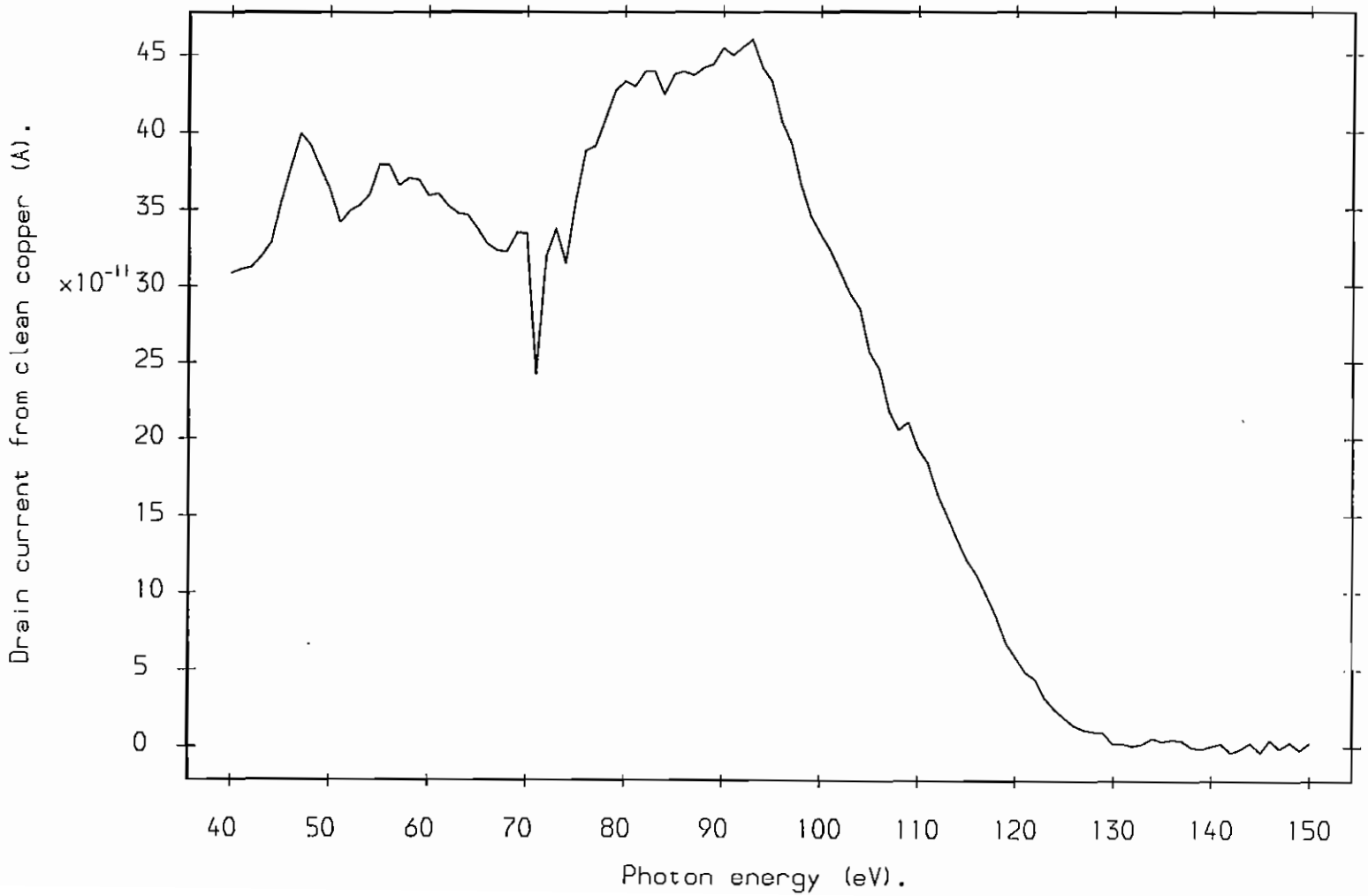

Figure 10.

30eV photon flux vs. SRS beam current.

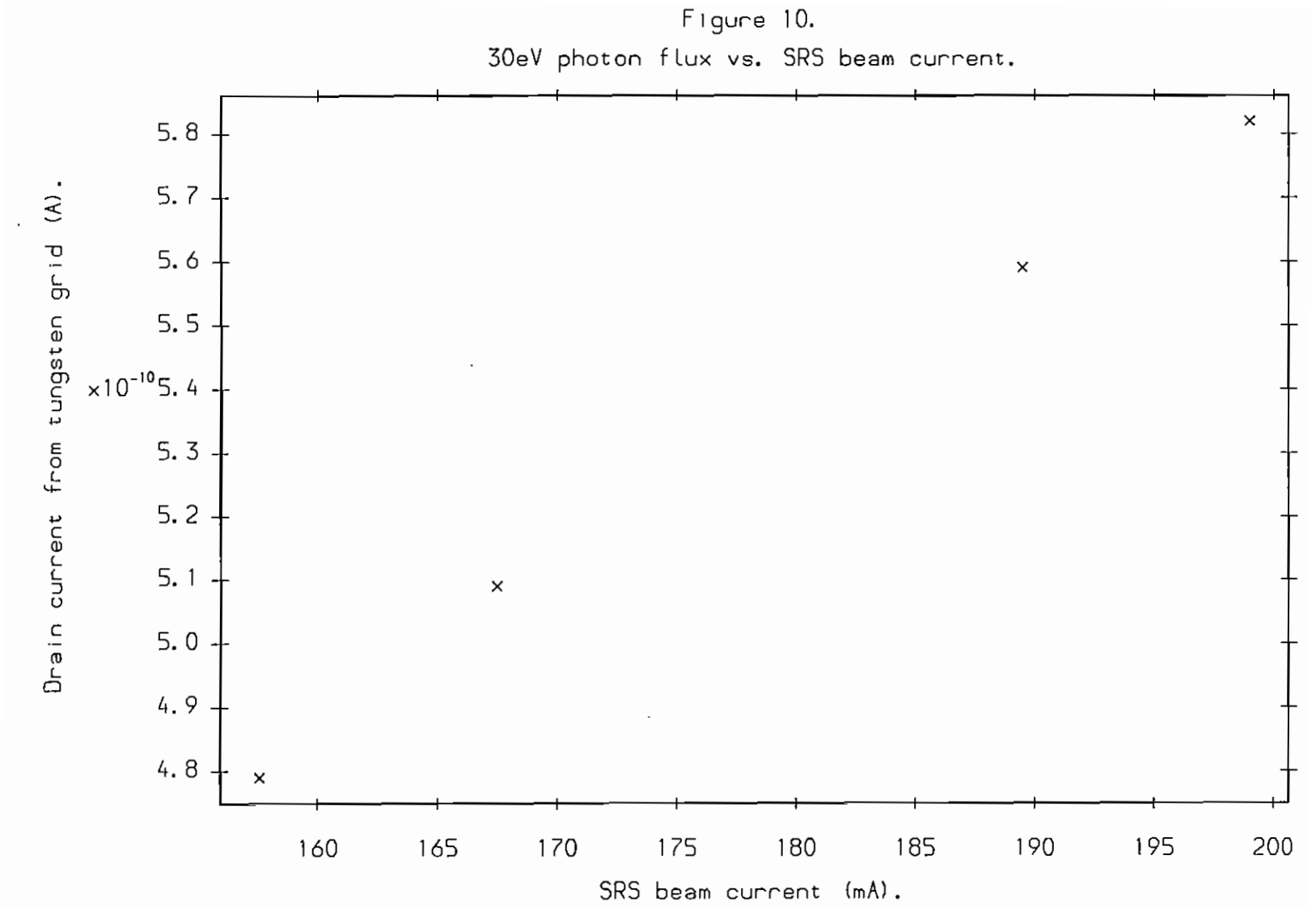

Figure 11.

I0 vs. Y1 micrometer after increasing exposure to beam.

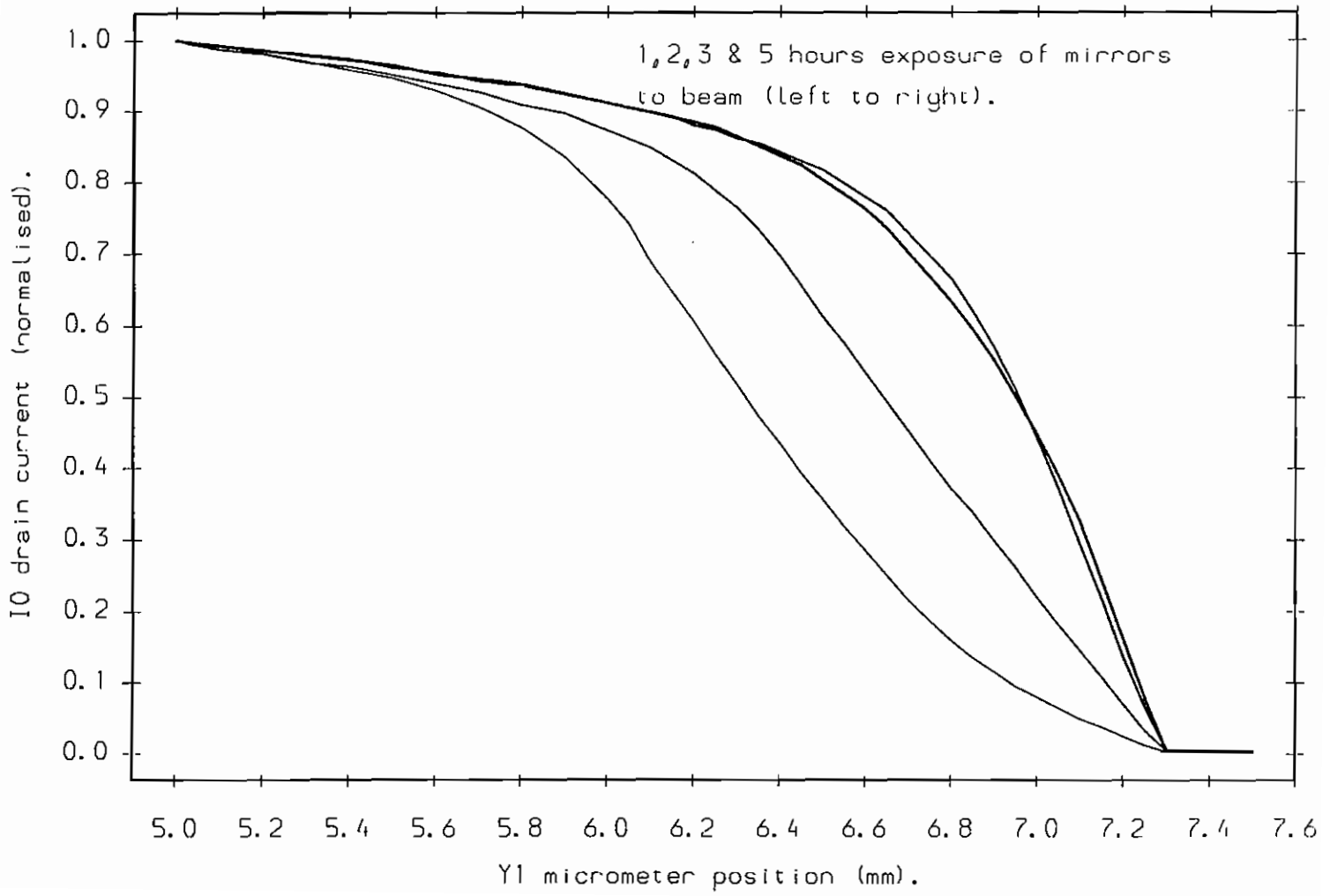

Figure 12.

Gl: k = 1,2 diffraction efficiency.

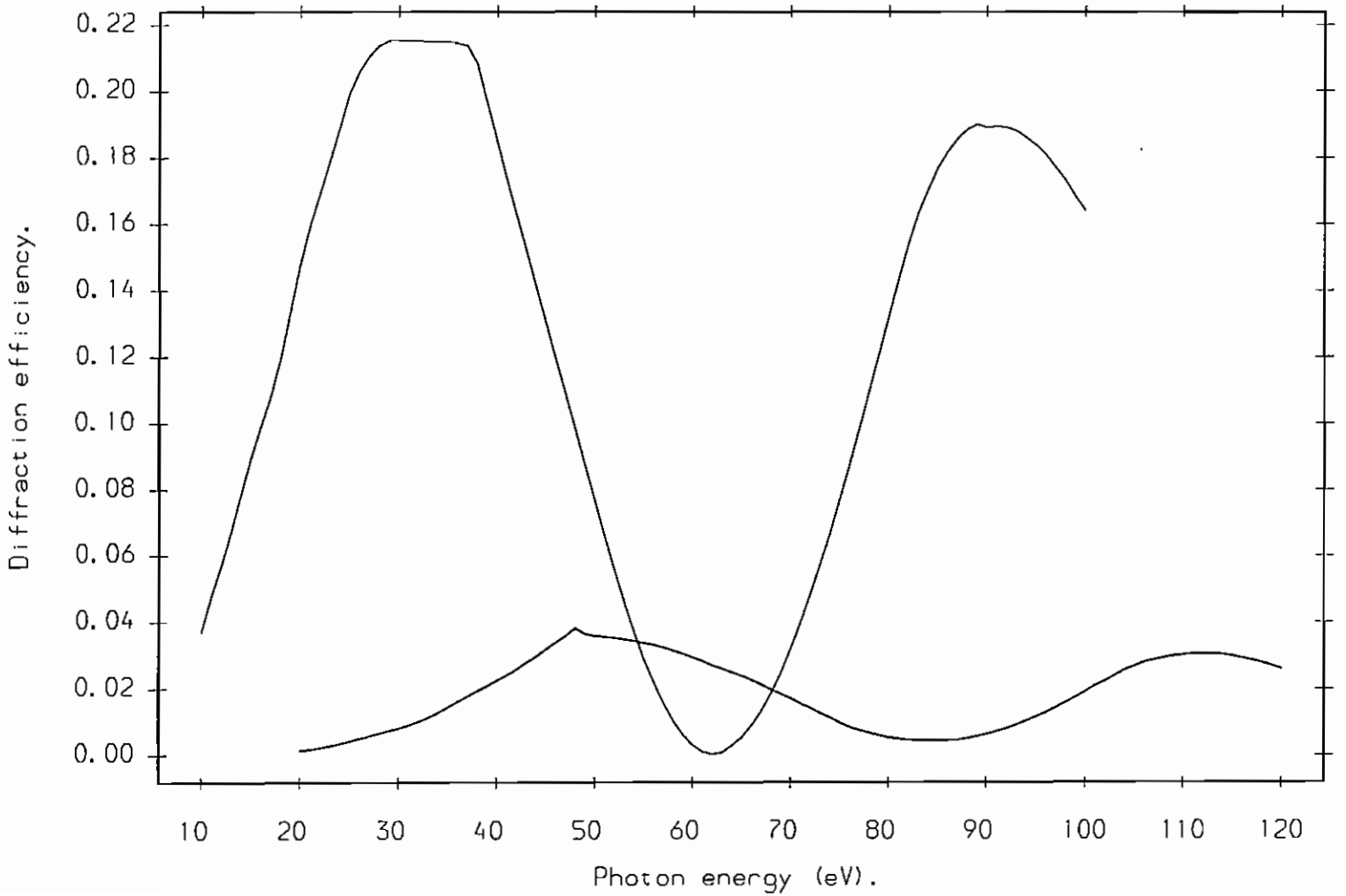

Figure 13.

G2: k = 1,2 diffraction efficiency.

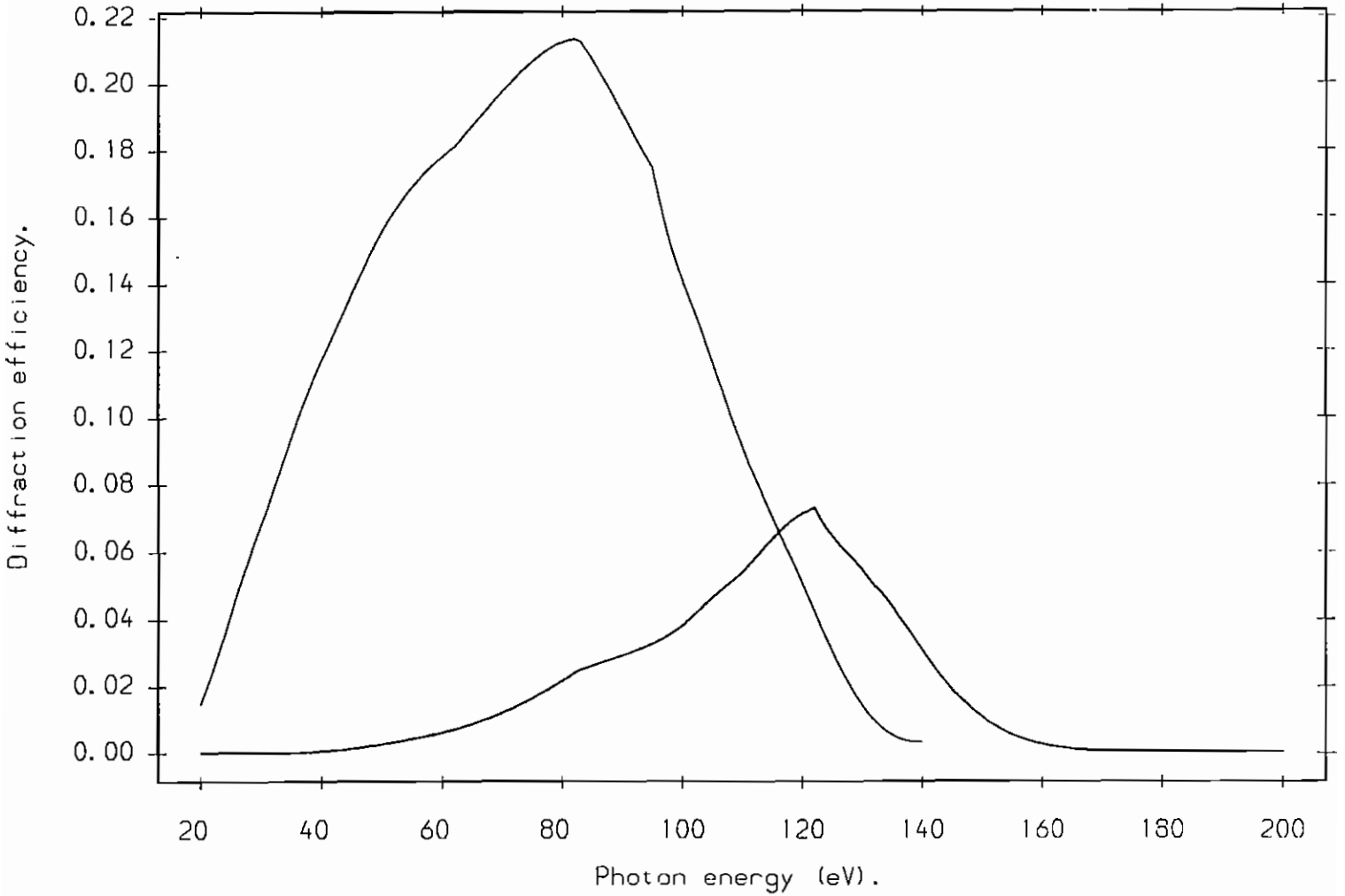

Figure 14.

G1 measured second order content.

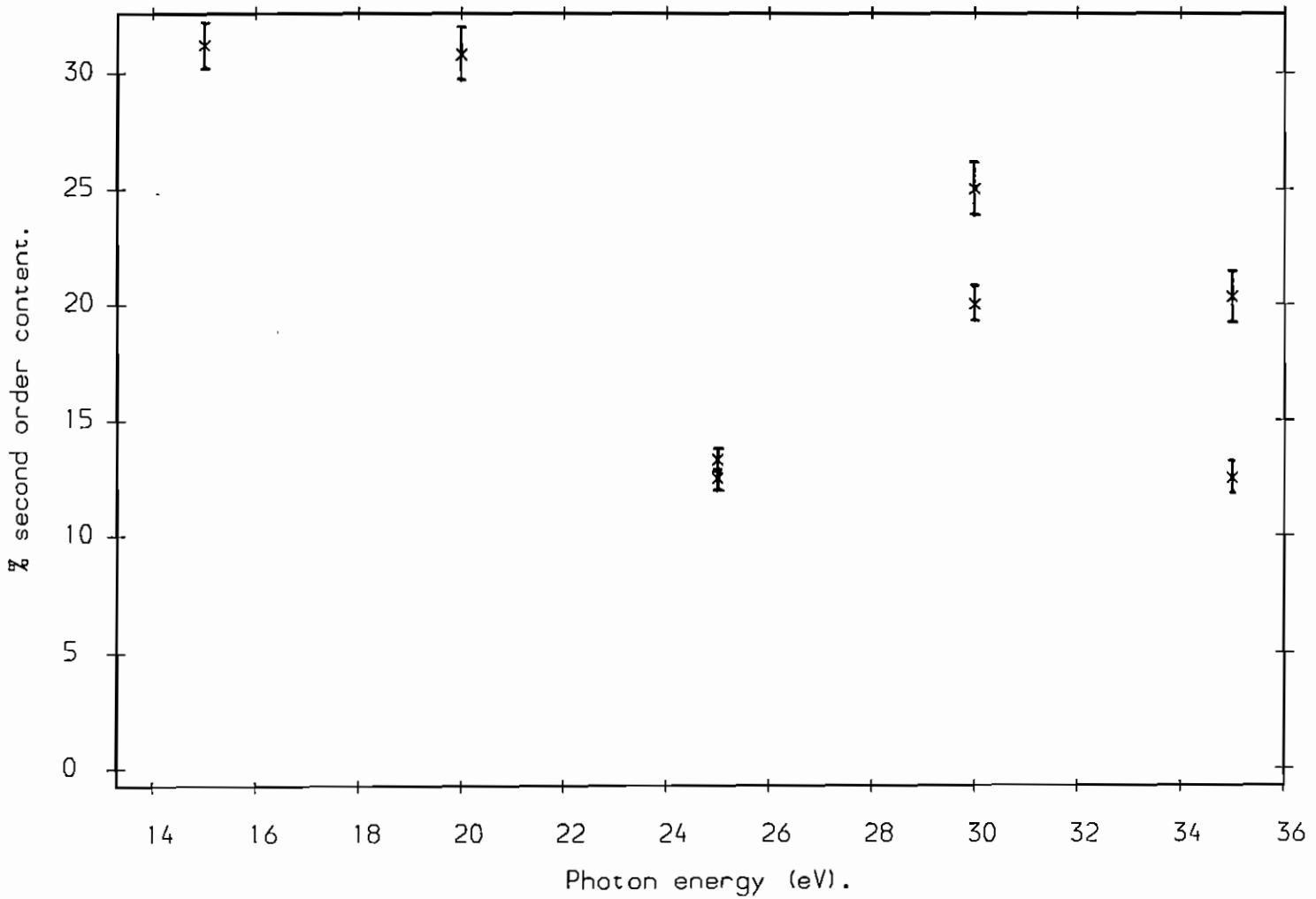

Figure 15.

G2 measured second order content.

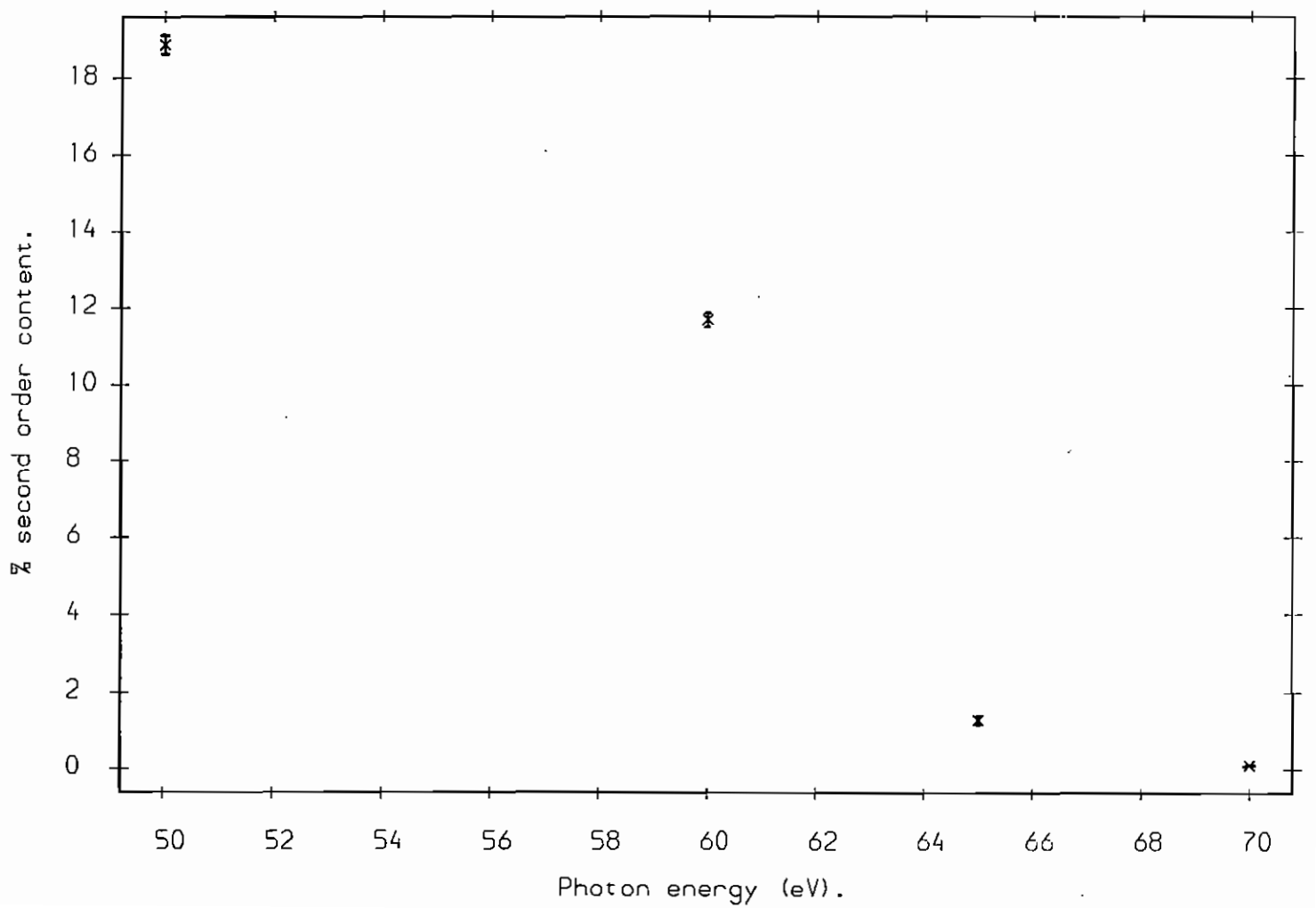

Figure 16.

Calculated entrance slit size contribution for S1=0.35mm: G1.

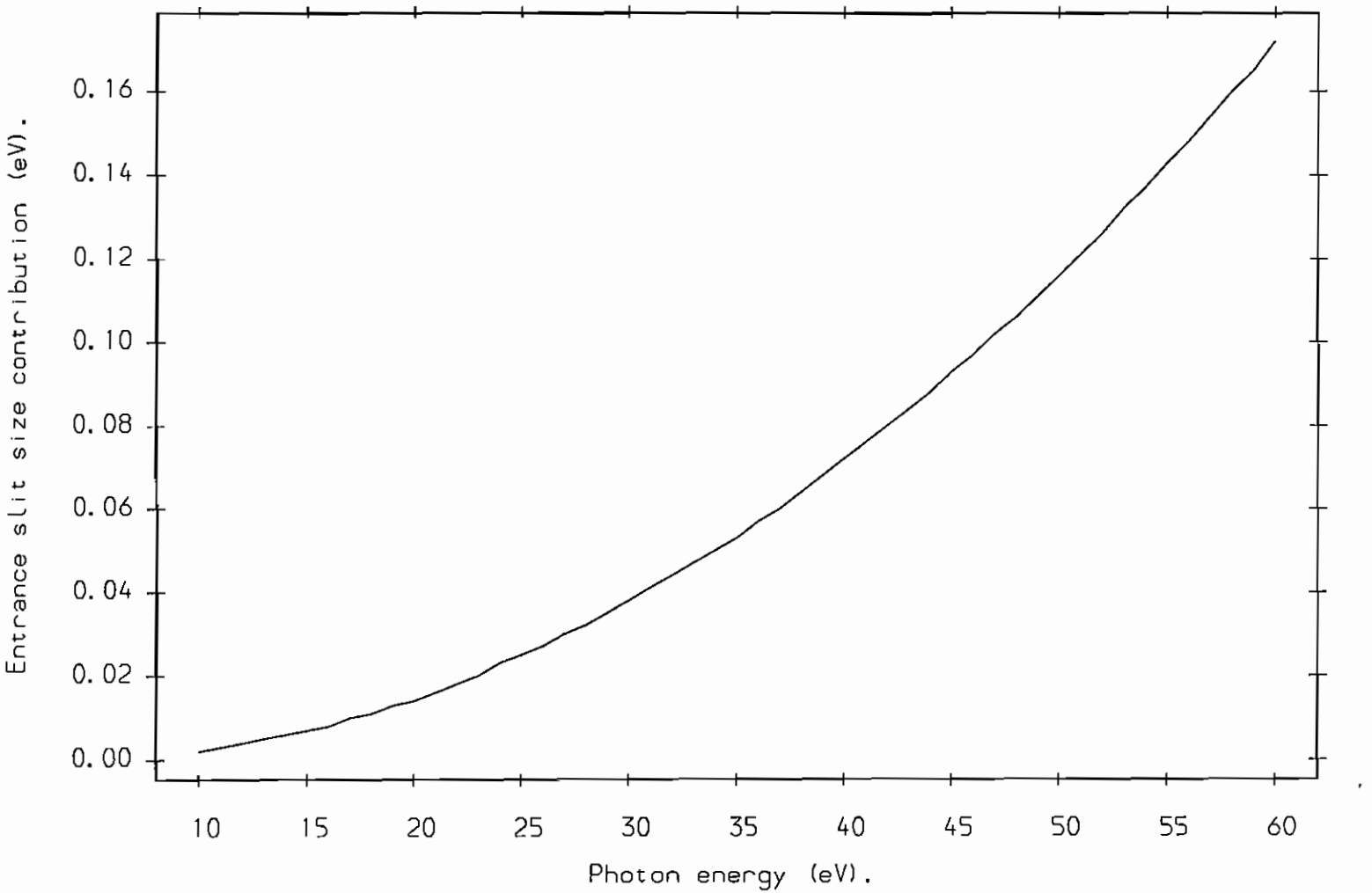

Figure 17.

Calculated entrance slit size contribution for S1=0.35mm: G2.

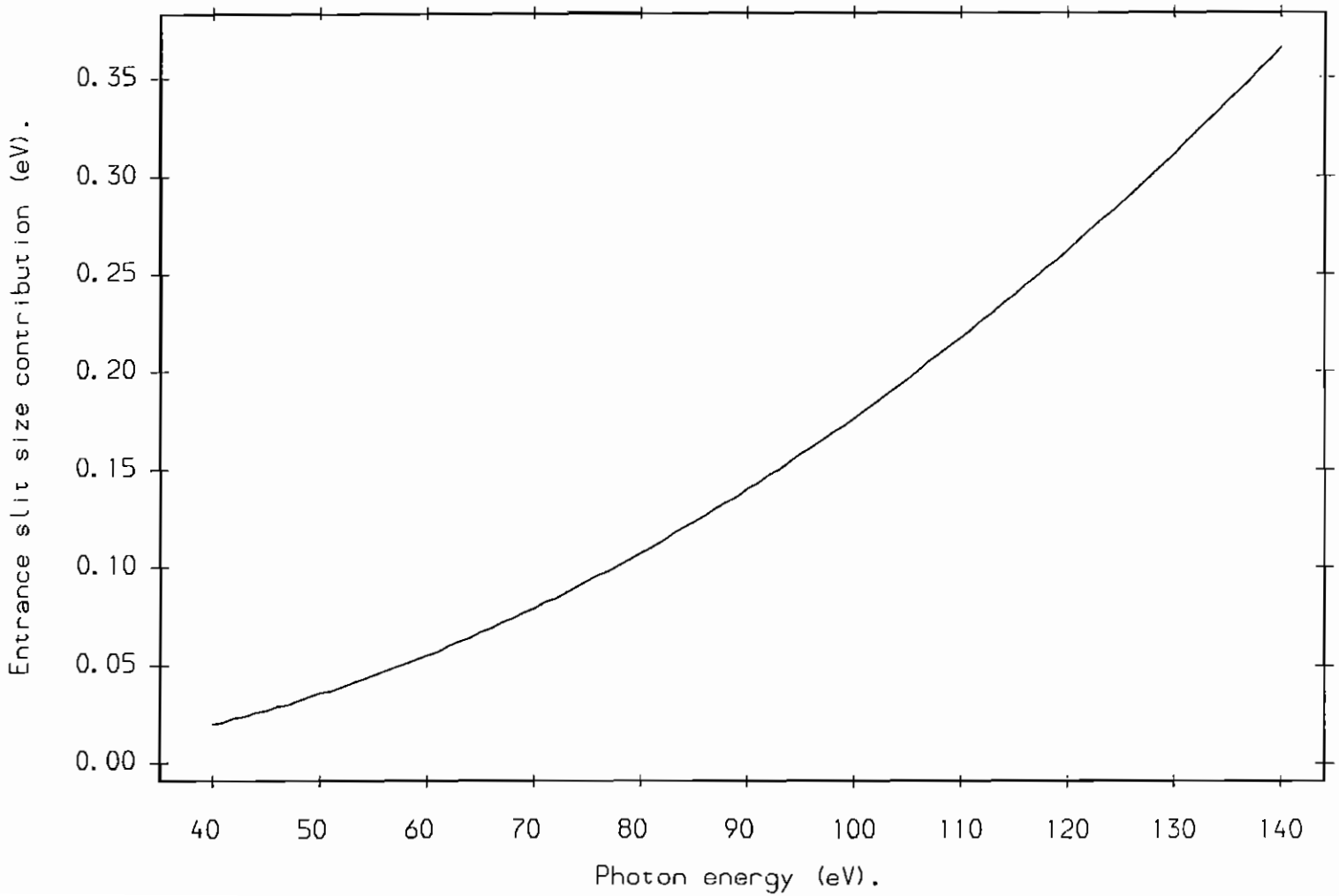

Figure 18.

Exit slit size for 0.1eV contribution, G1.

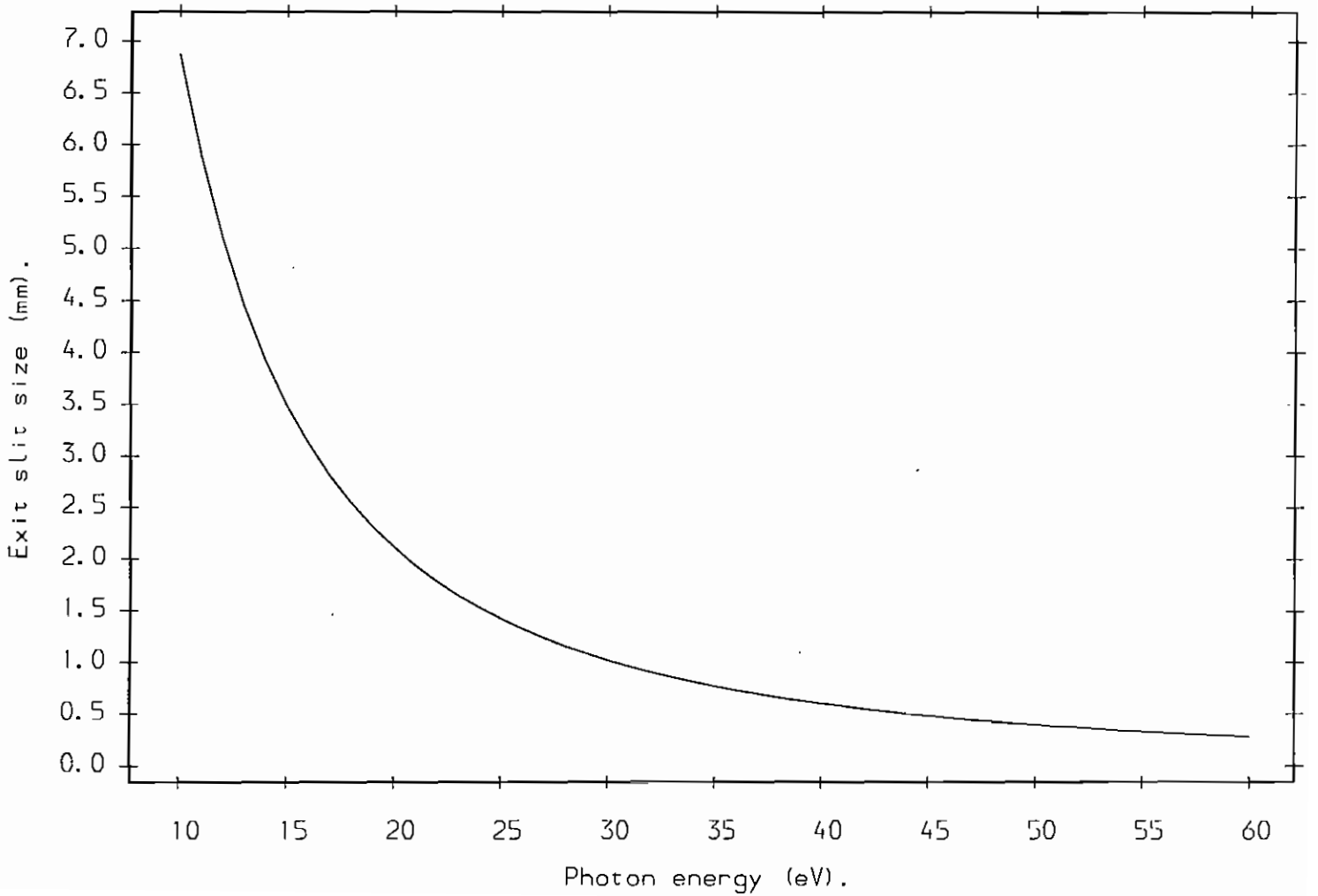

Figure 19.

Exit slit size for 0.1eV contribution, G2.

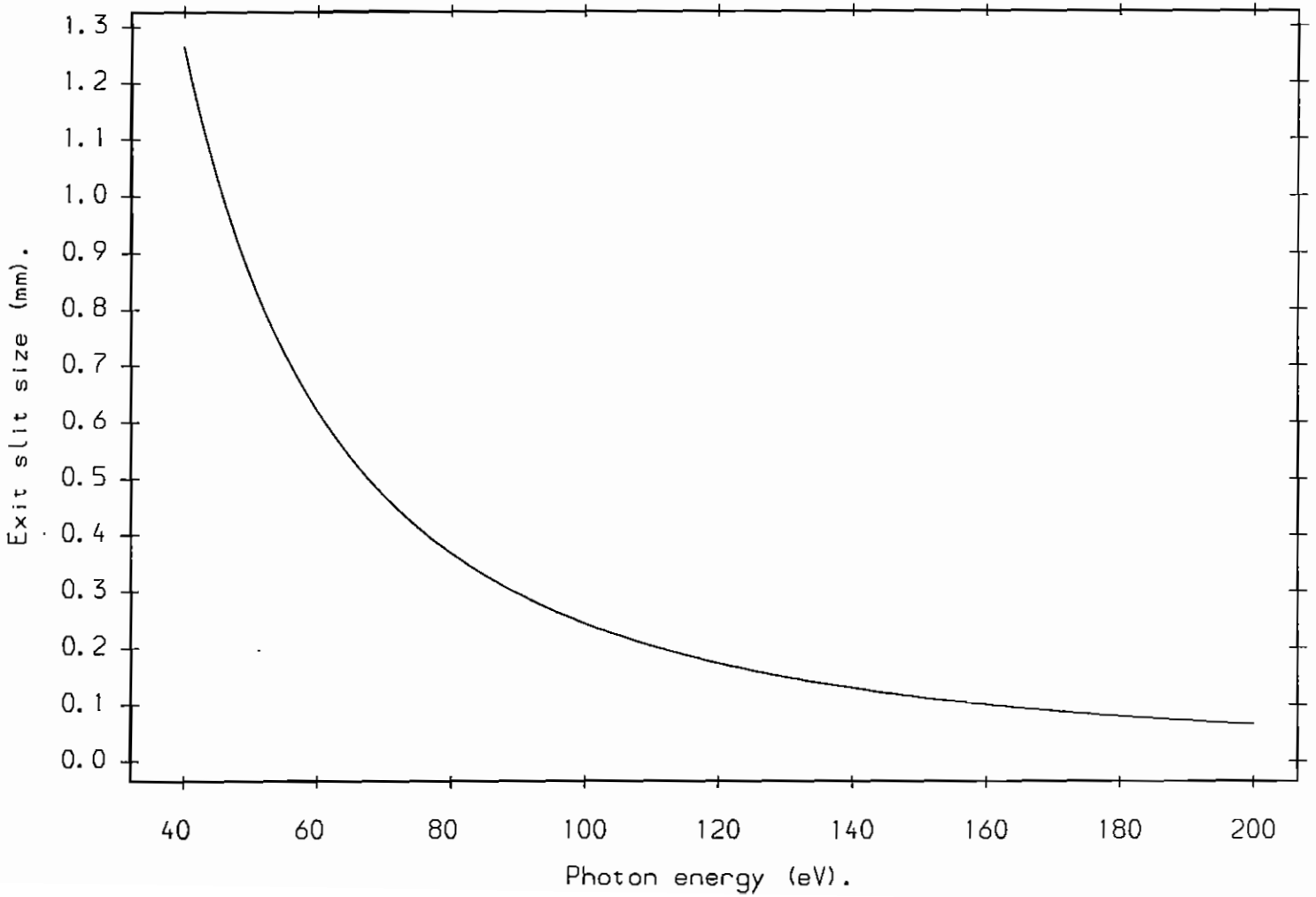

Figure 20.

Calculated geometrical aberration contribution, G1.

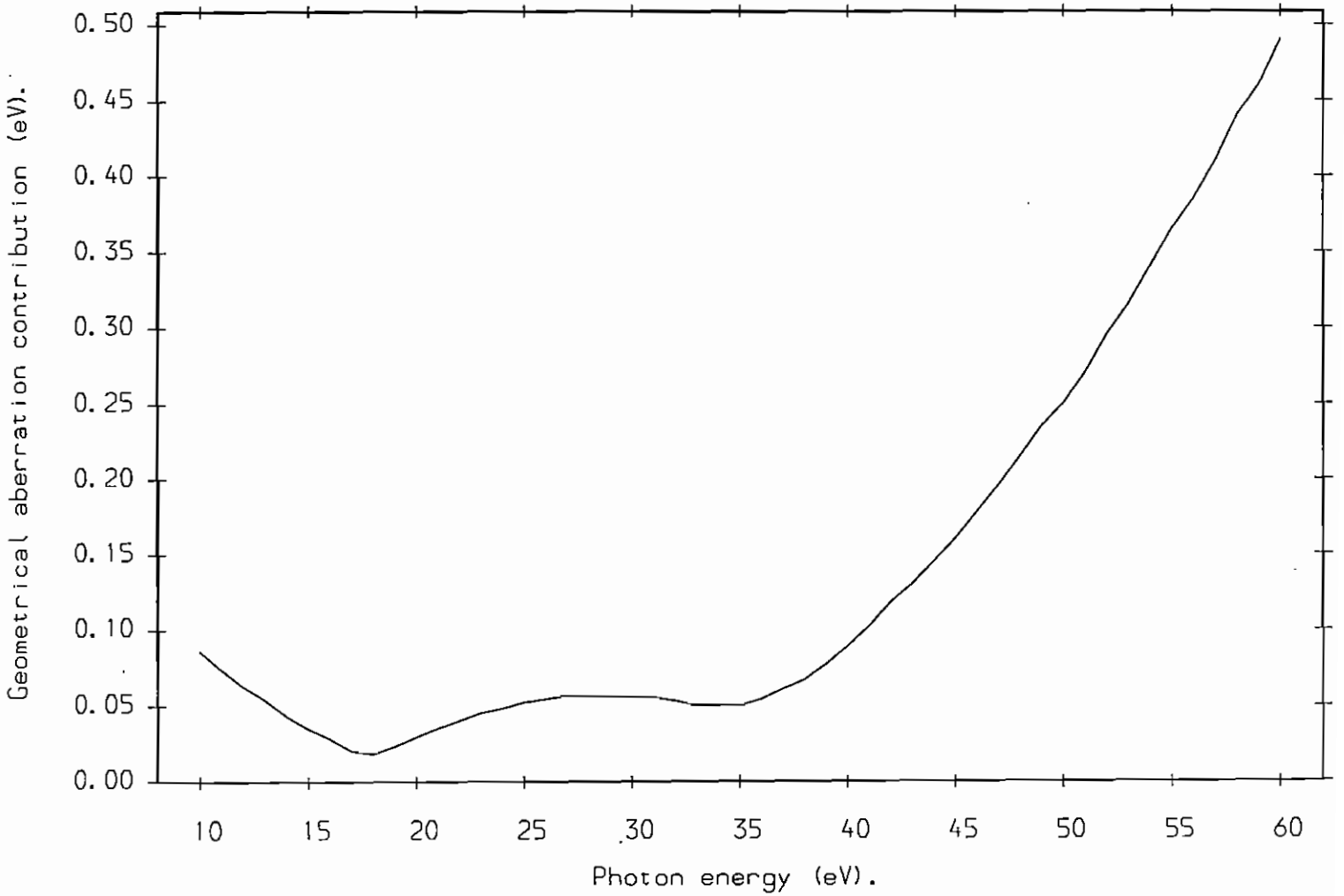

Figure 21.

Calculated geometrical aberration contribution, G2.

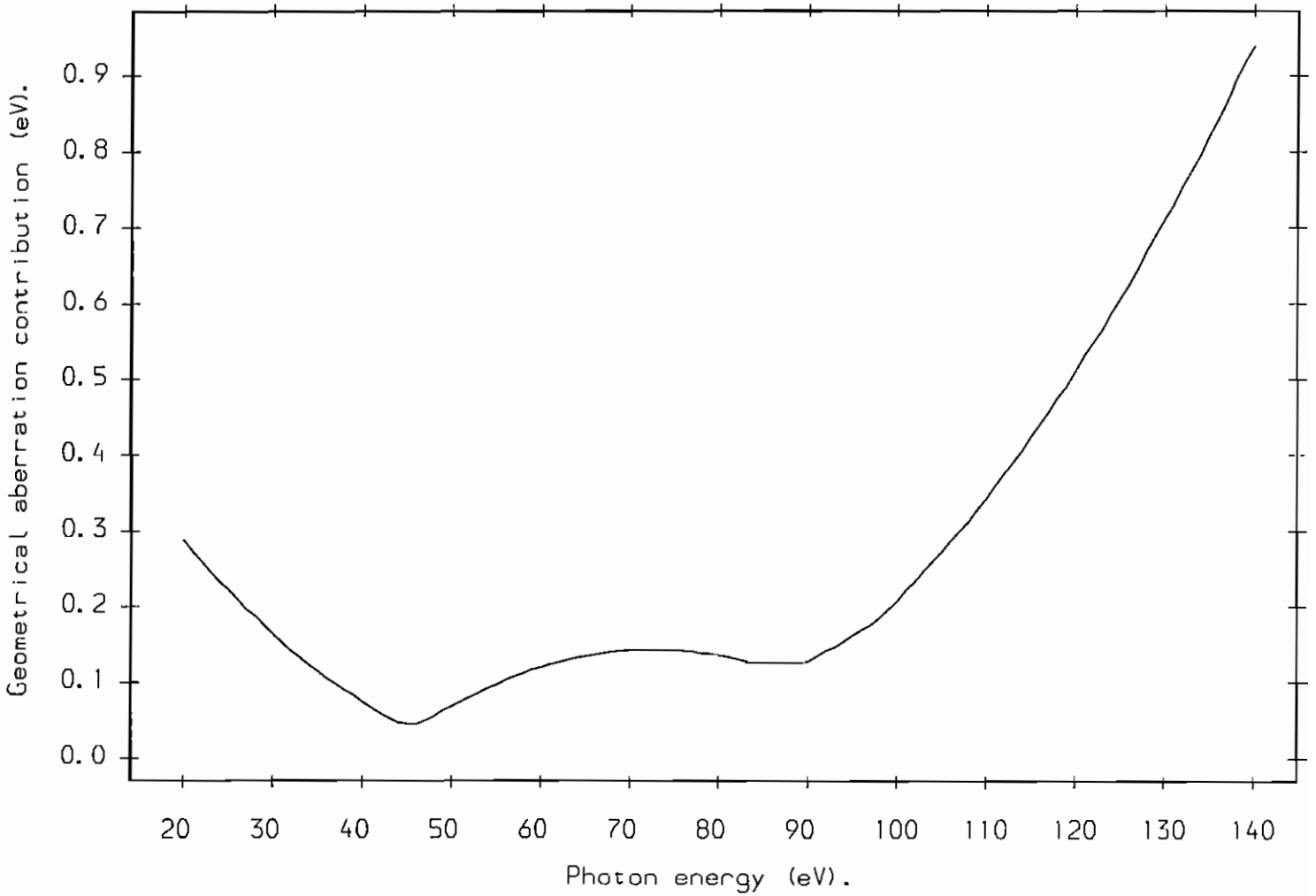

Figure 22.

Measured and theoretical analyser resolution.

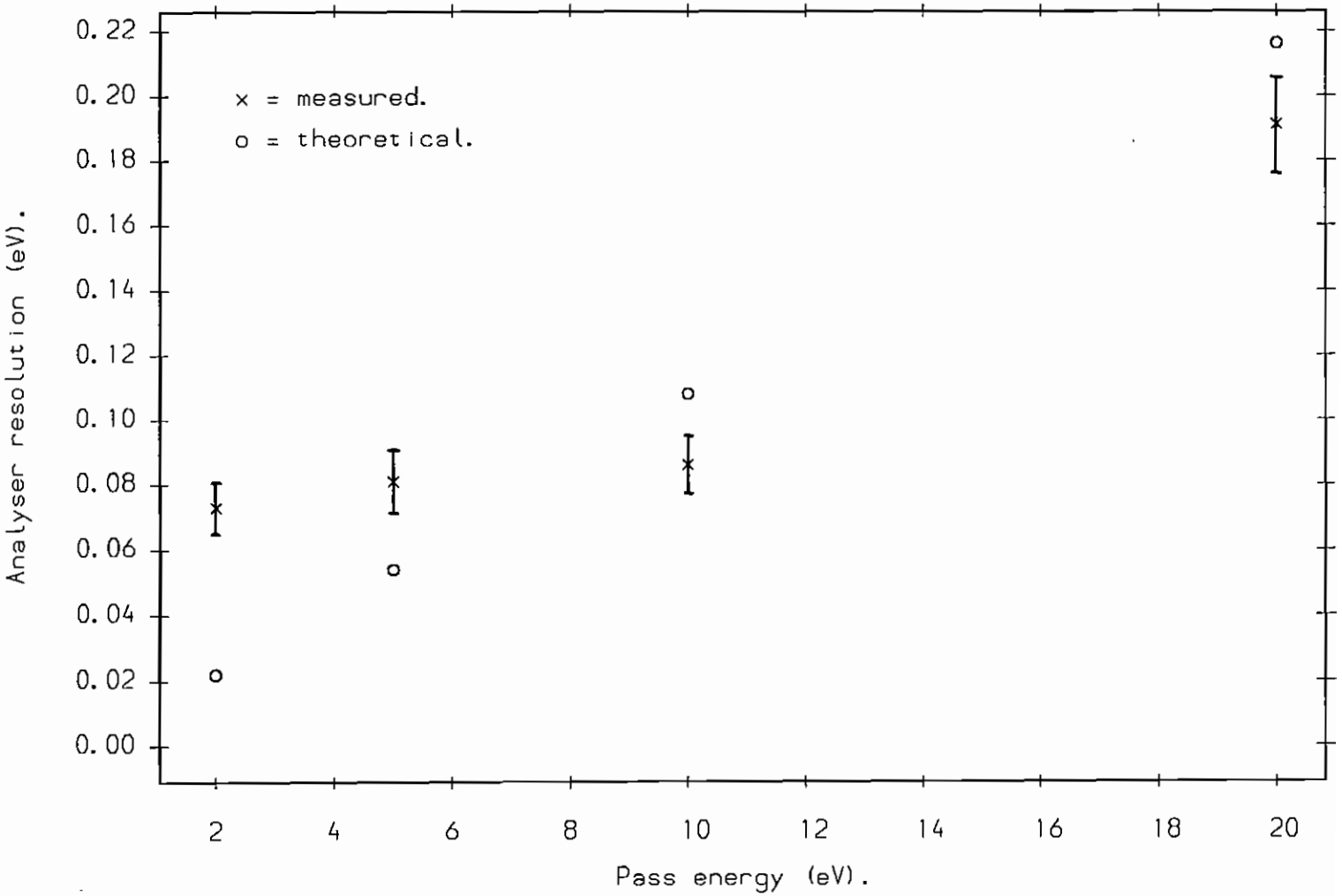

Figure 23.

Intensity vs. analyser pass energy.

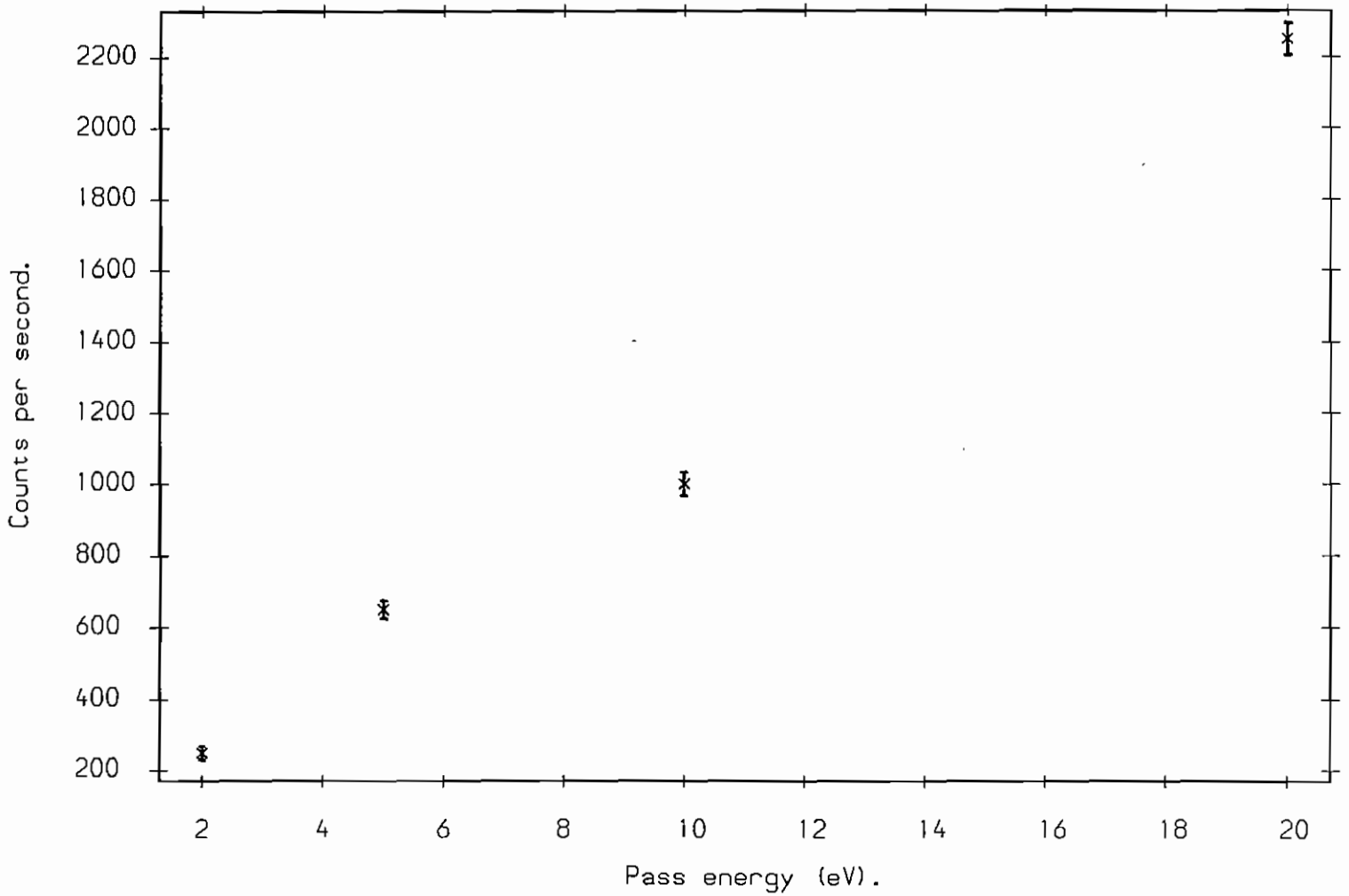

Figure 24.

Fermi edge position vs. pass energy.

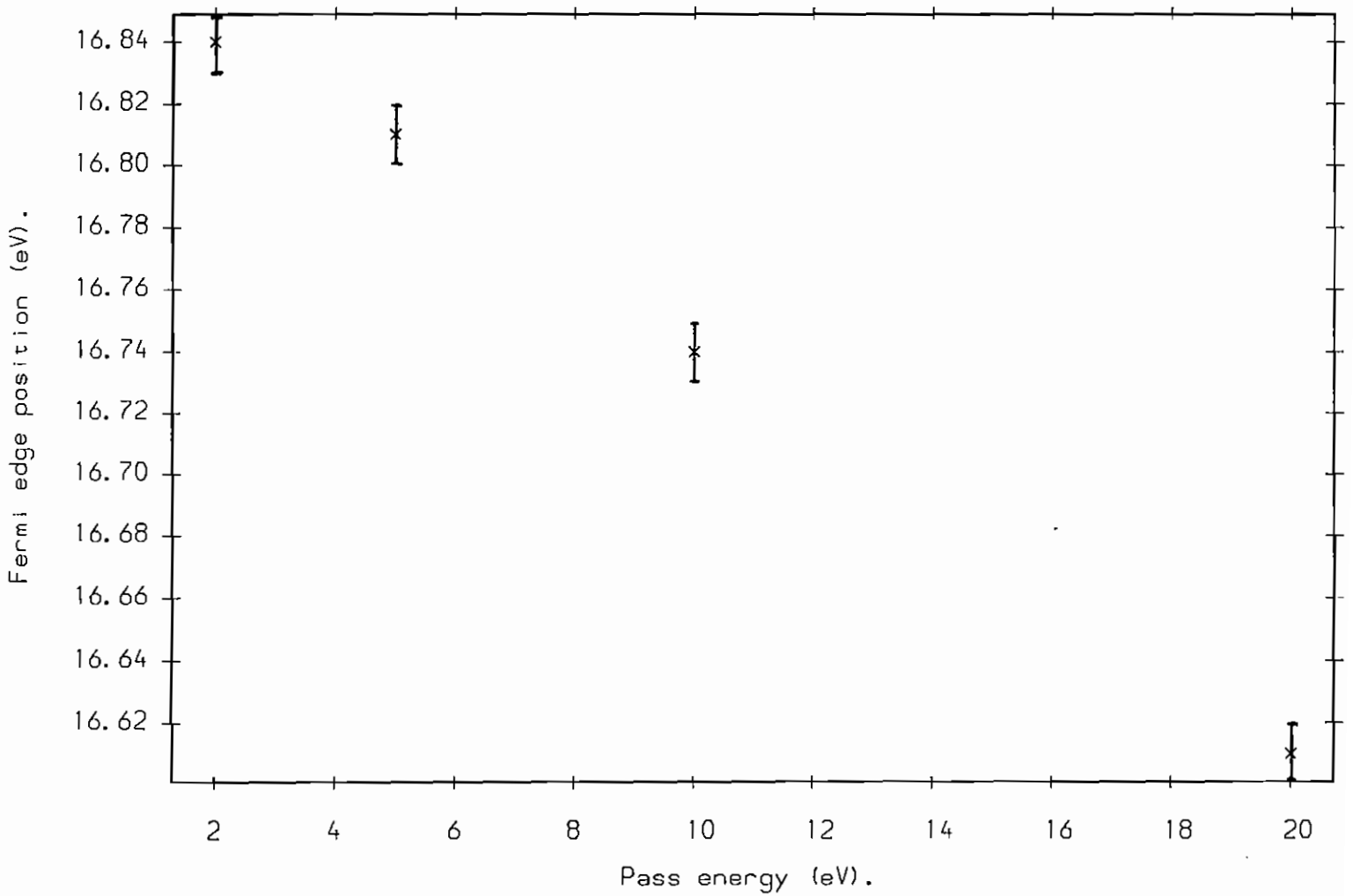

Figure 25.

Tantalum Fermi edge, 18eV photon energy, raw data.

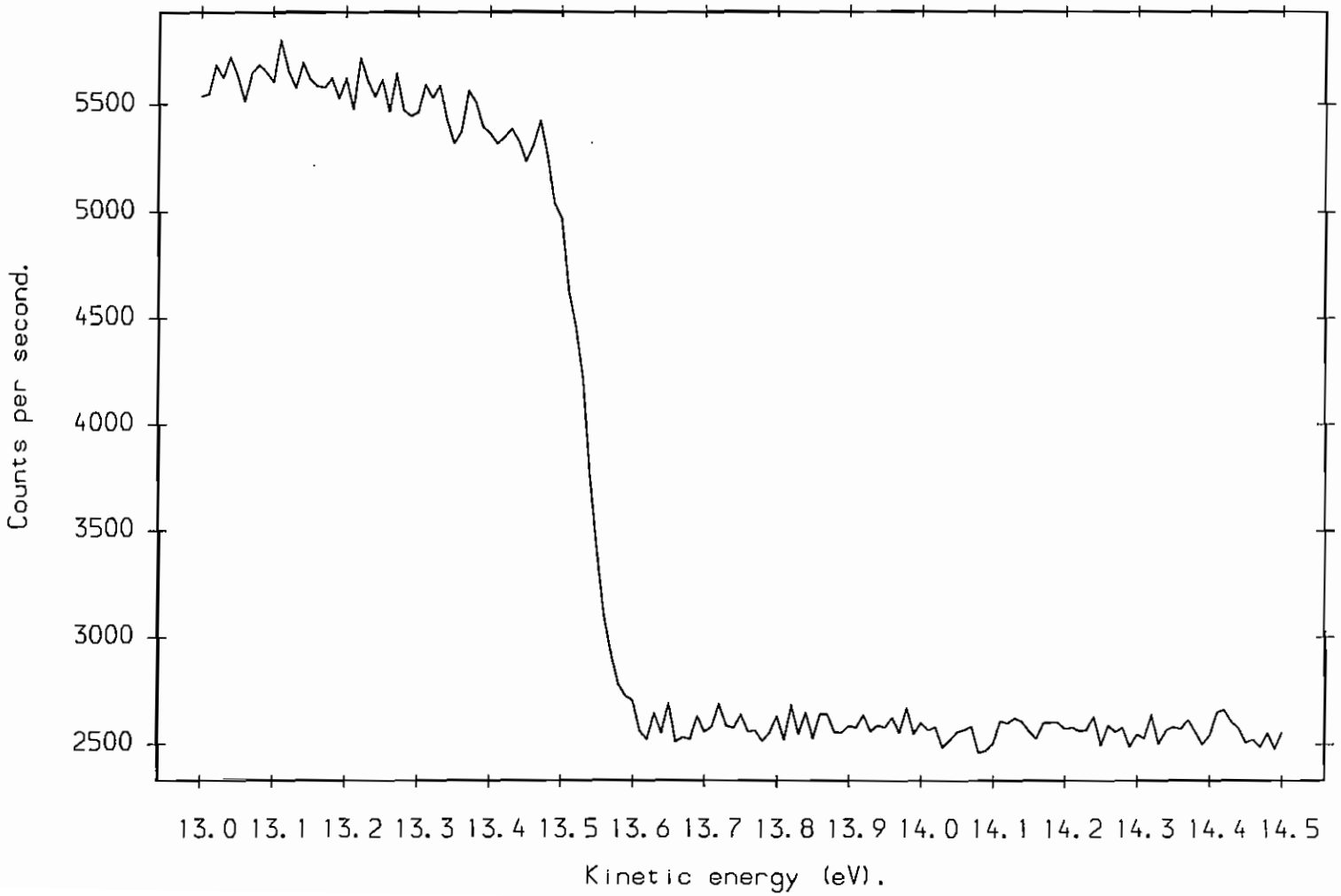

Figure 26.

Calculated monochromator contribution, G1.

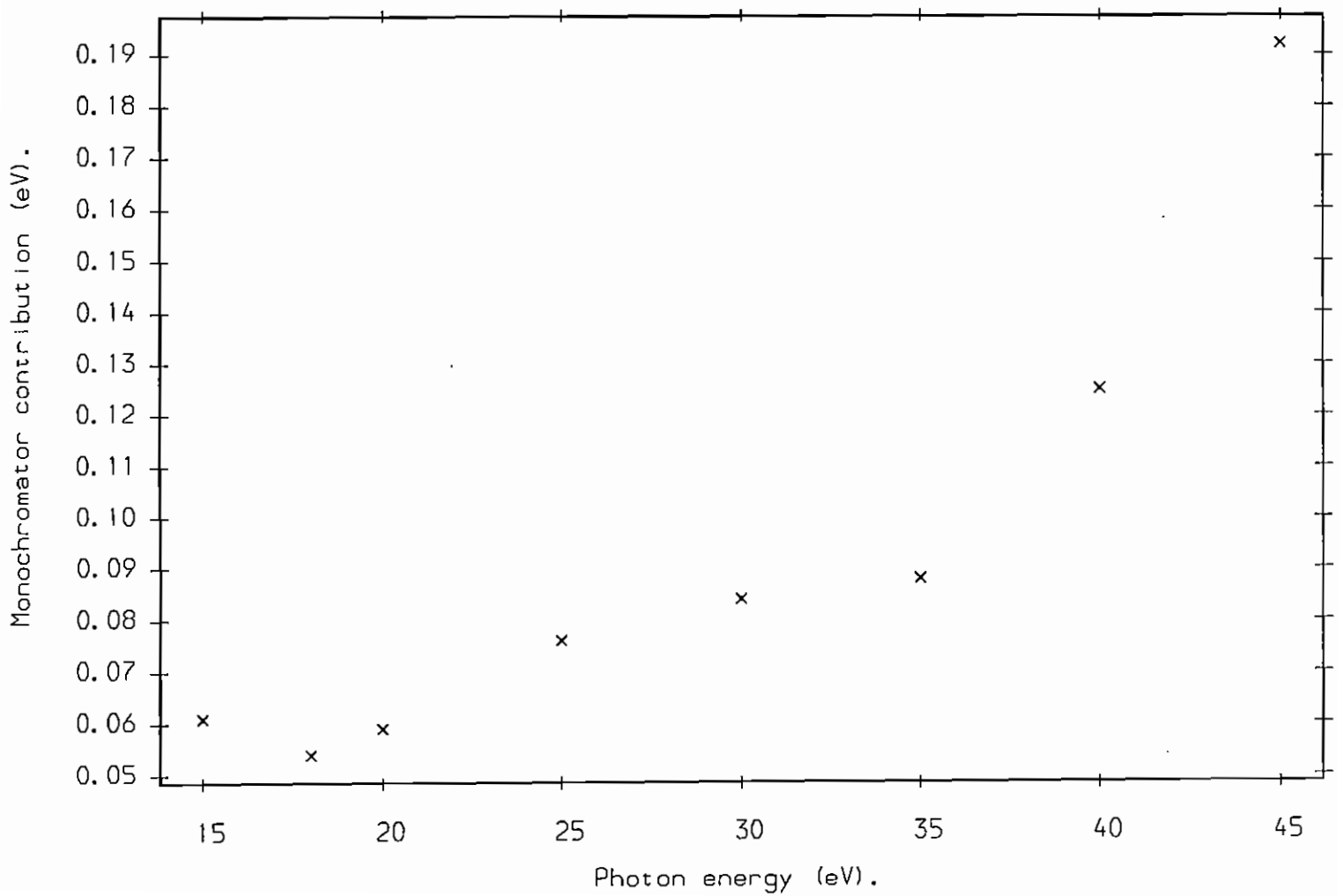

Figure 27.

Measured and expected FWHM, G1.

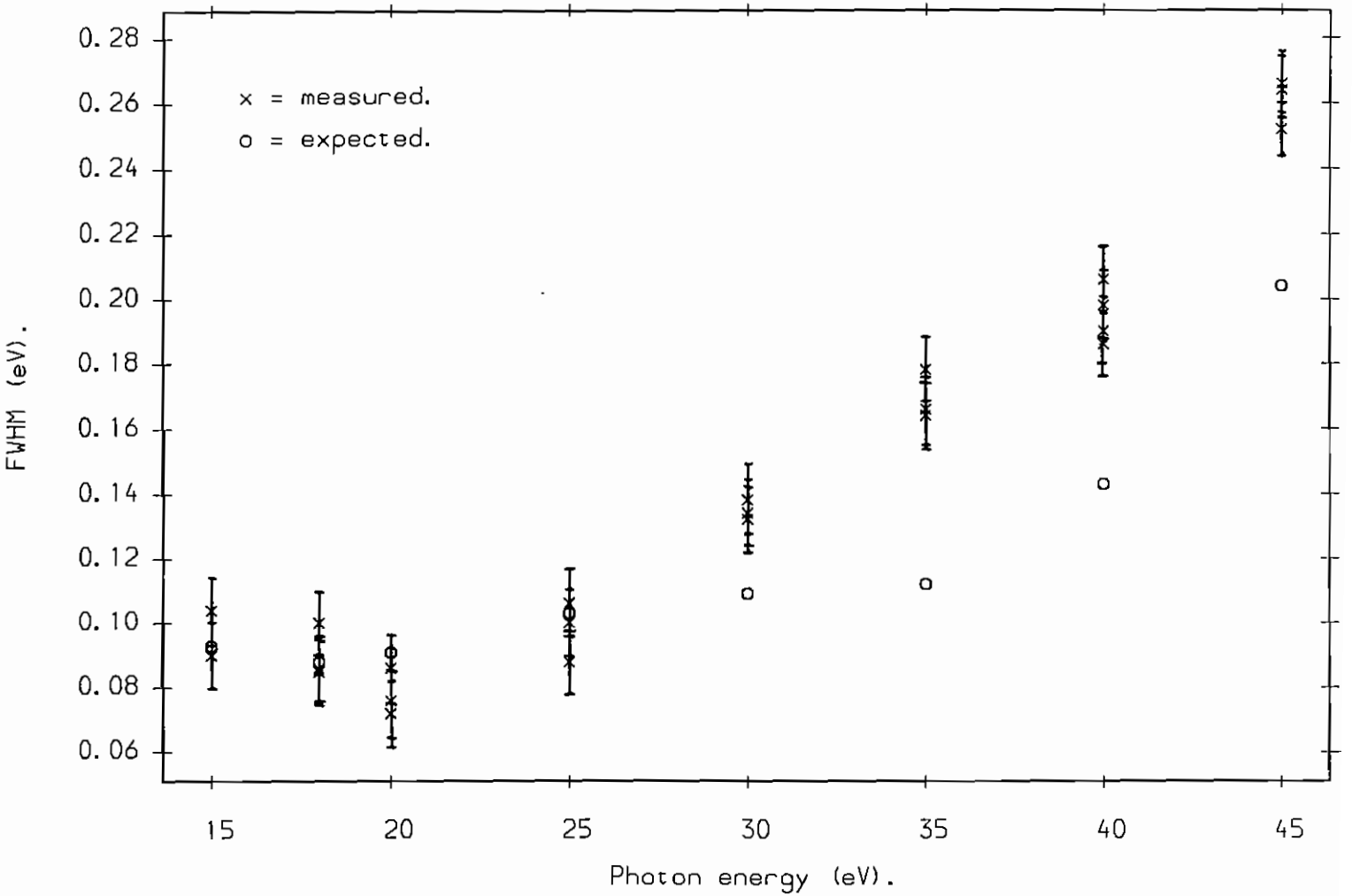

Figure 28.

Measured and expected FWHM, G1 (r=1.9m).

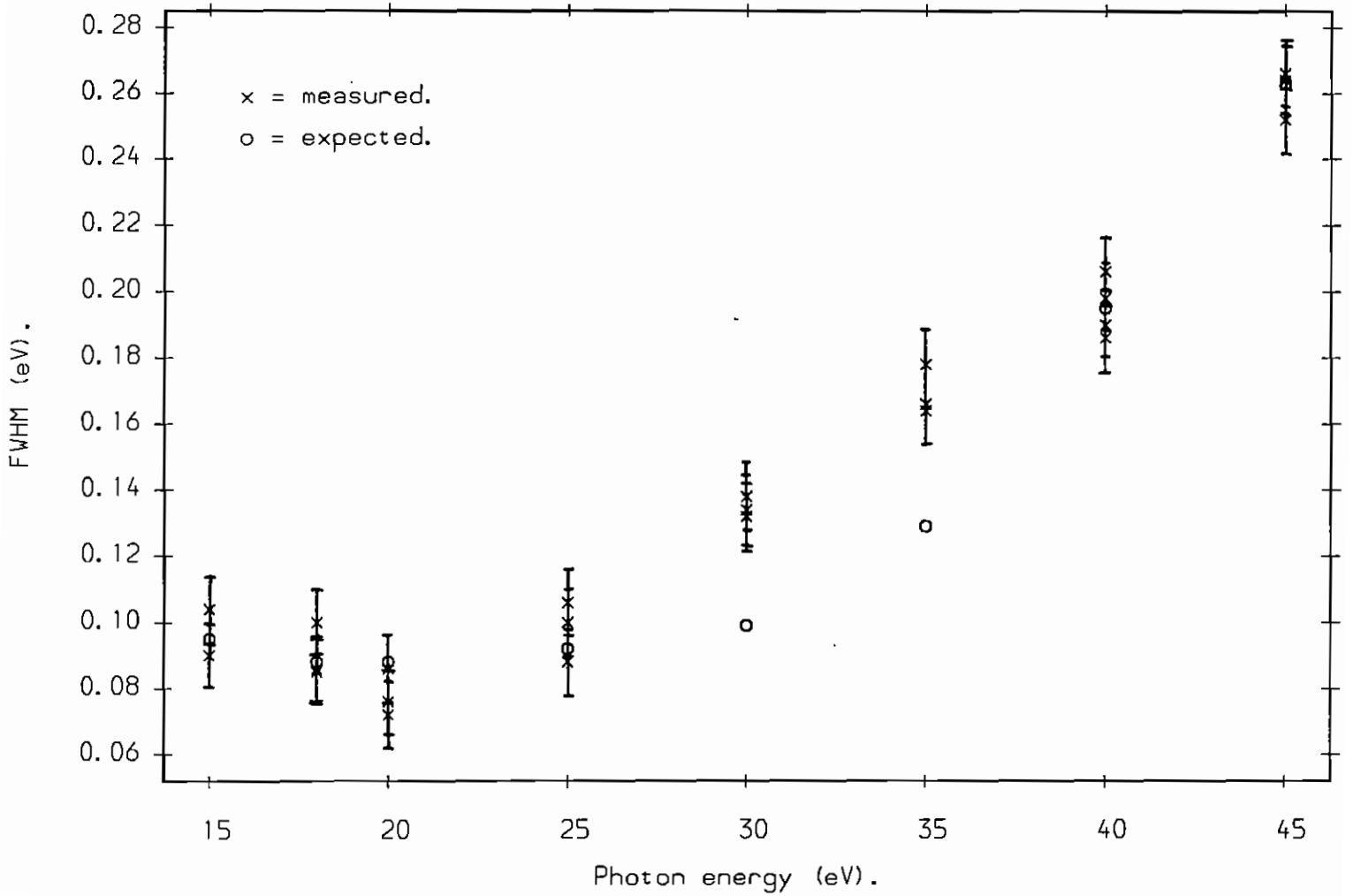

Figure 29.

Calculated monochromator contribution, G2.

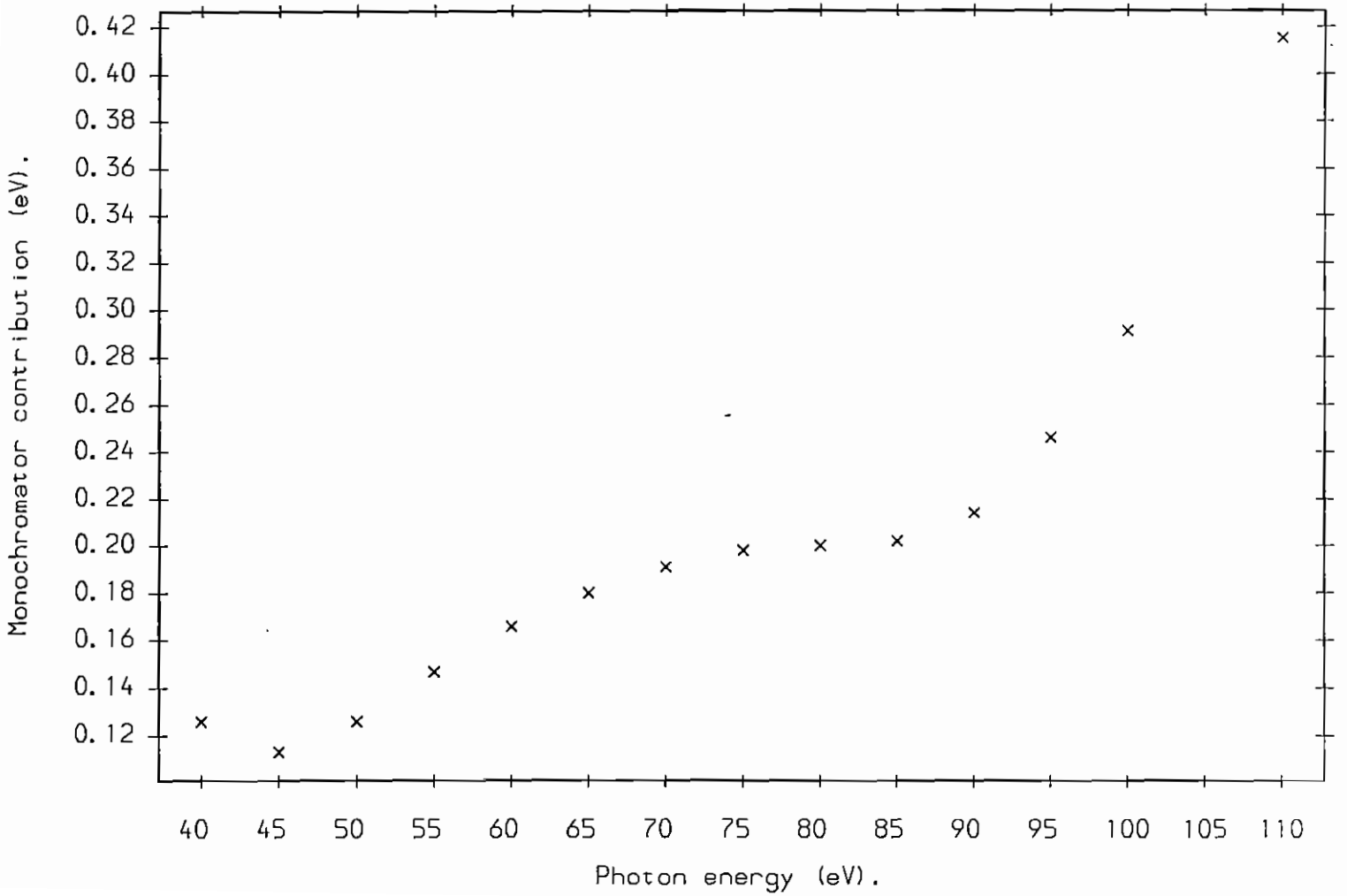

Figure 30.
Measured and expected FWHM, G2.

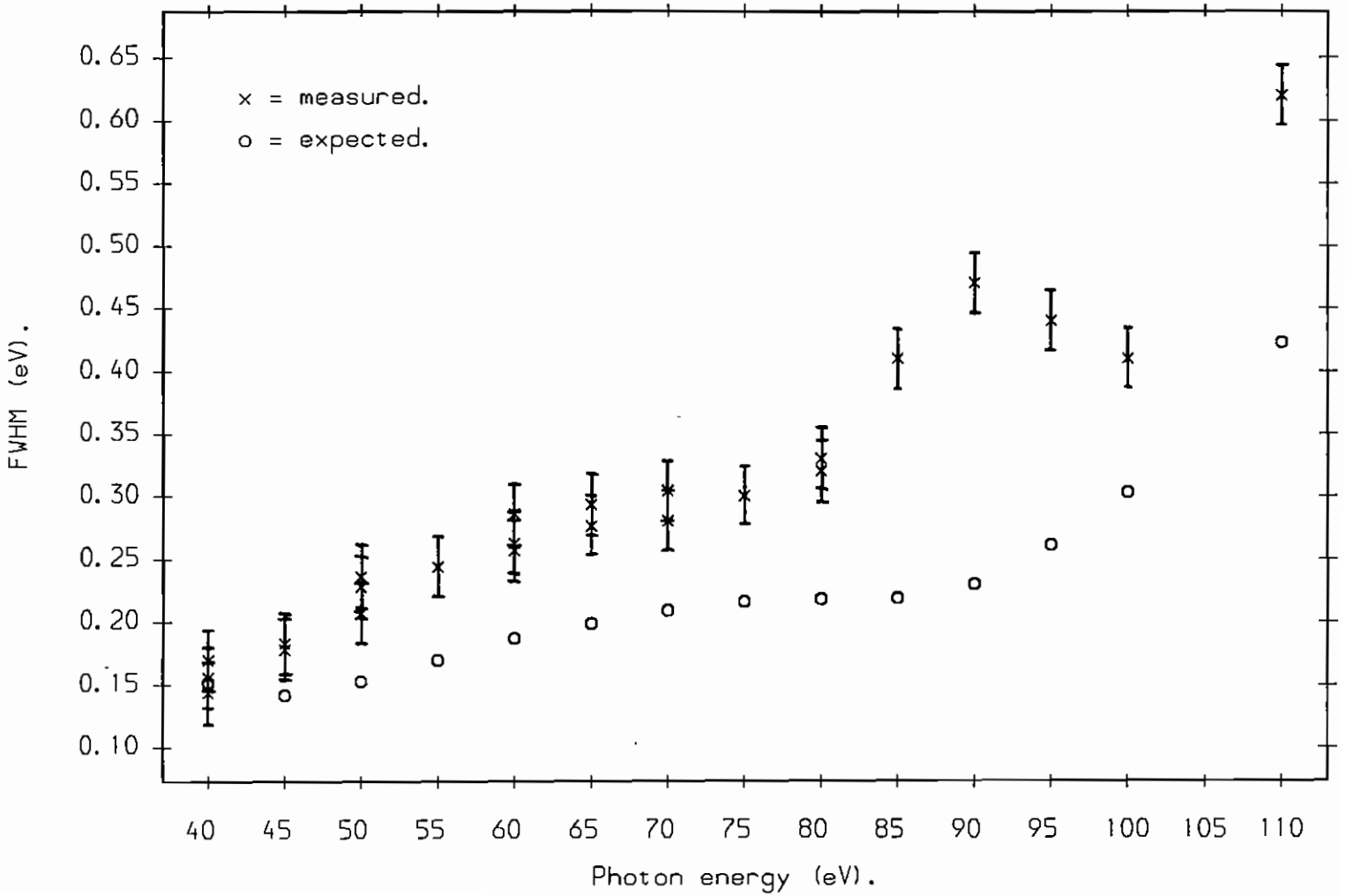

Figure 31.

Measured and expected FWHM, G2 (r=1.9m, R=9.8m).

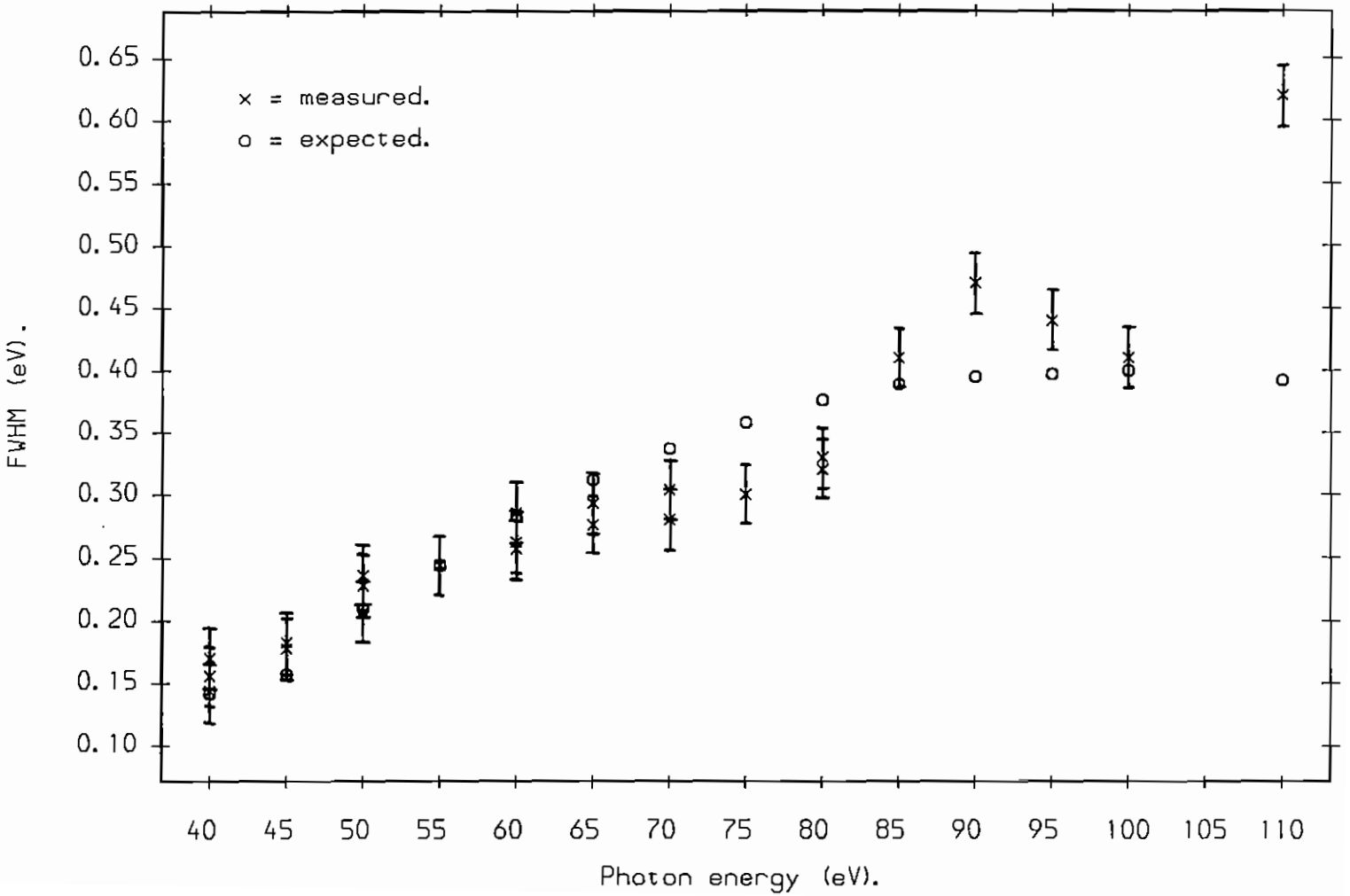

Figure 32.

Measured FWHM, Y1 = 5mm and 7mm.